



## Evaluation of Earth Observation based global long term vegetation trends – Comparing GIMMS and MODIS global NDVI time series

Rasmus Fensholt\*, Simon R. Proud

*Department of Geography and Geology, University of Copenhagen, Øster Voldgade 10, DK-1350 Copenhagen, Denmark*

---

### ARTICLE INFO

**Article history:**

Received 6 June 2011

Received in revised form 12 December 2011

Accepted 22 December 2011

Available online 25 January 2012

---

**Keywords:**

NDVI

Linear trend analysis

Terra and Aqua MODIS

AVHRR GIMMS3g

Global scale

---

### ABSTRACT

A new and updated version of the AVHRR (Advanced Very High Resolution Radiometer) based GIMMS (Global Inventory Modelling and Mapping Studies) NDVI (Normalized Difference Vegetation Index) dataset is now available covering 1981 to 2010 (GIMMS3g). Earlier versions of this global coverage 15-day composite dataset have been used for numerous local to global scale vegetation time series studies during recent years. However, several aspects of the AVHRR sensor design and data processing potentially introduce substantial noise into the NDVI dataset if not corrected for. The more recent NDVI dataset from Terra MODIS (Moderate Resolution Imaging Spectroradiometer) is considered an improvement over AVHRR data and with the release of GIMMS3g an overlapping period of 11 years now provides a possibility to perform a robust evaluation of the accuracy of GIMMS3g data and derived trends. In this study the accuracy is evaluated by comparison with the global Terra MODIS NDVI (MOD13C2 Collection 5) data using linear regression trend analysis. The trends of GIMMS NDVI were found to be in overall acceptable agreement with MODIS NDVI data. A significant trend in NDVI ( $\alpha = 0.05$ ) was found for 11.8% of the MODIS NDVI pixels on a global scale (5.4% characterised by positive trends and 6.3 with negative trends) whereas GIMMS NDVI analysis produced a total of 10.5% significant pixels (4.9% positive, 5.6% negative). However, larger differences were found for the Southern Hemisphere land masses (South America and Australia) and the high northern latitude Arctic regions. From a linear regression analysis the correlation coefficient between the two datasets was found to be highly significant for areas with a distinct phenological cycle. Discrepancies between the GIMMS and MODIS datasets were found in equatorial areas (broadleaved, evergreen forest), Arctic areas (sparse herbaceous or sparse shrub cover) and arid areas (herbaceous cover, closed-open). Linear regression of QA filtered Terra and Aqua MODIS NDVI (2003–2010) revealed similar inconsistencies for Arctic and equatorial areas suggesting that robust long-term NDVI trend estimates in these areas are difficult to obtain from both GIMMS and MODIS data. Additionally, GIMMS based NDVI trend analysis in arid areas of limited photosynthetic activity should be interpreted with caution. The regression coefficient (slope value) ( $p < 0.01$ ) was found to be close to 1 for most land cover types on a global scale (global land cover class average slope = 1.00) suggesting overall compatibility between MODIS and GIMMS NDVI, but with land cover class specific variations (within class and between classes).

© 2012 Elsevier Inc. All rights reserved.

---

### 1. Introduction

Our understanding of variations in vegetation resources from a local to global scale has improved by quantifying inter-annual trends in vegetation from time series of Advanced Very High Resolution Radiometer (AVHRR) data covering the last three decades (from 1981 to present). AVHRR NDVI has been widely used for regional to global scale vegetation trend analysis (Anyamba & Tucker, 2005; de Jong et al., 2011; Eklundh & Olsson, 2003; Hellden & Tottrup, 2008; Jeyaseelan et al., 2007; Myneni et al., 1998; Olsson et al., 2005; Slayback et al., 2003; Tucker et al., 2001) and changes in vegetation

phenology (Heumann et al., 2007; Myneni et al., 1997; Stockli & Vidale, 2004). Other studies of AVHRR NDVI time series have examined the response of vegetation vigour to climatic variations of variables like rainfall and air temperature to understand causes of observed changes in vegetation greenness (Fensholt & Rasmussen, 2011; Herrmann et al., 2005; Zeng et al., 2005). AVHRR NDVI has also been used as input for terrestrial NPP (Net Primary Production) estimates (Hickler et al., 2005; Prince & Goward, 1995; Ruimy et al., 1994) with Nemani et al. (2003) using two different AVHRR NDVI global coverage products as input for NPP modelling to analyse climate driven changes in global terrestrial NPP.

The AVHRR sensors were not originally intended for vegetation study (Cracknell, 2001) using indices like NDVI (Rouse et al., 1973). When the potential and shortcomings of AVHRR for vegetation studies became a subject of research (Holben, 1986; Tucker et al., 1983)

\* Corresponding author. Fax: +45 35322501.

E-mail address: [rf@geo.ku.dk](mailto:rf@geo.ku.dk) (R. Fensholt).

modifications to optimise the sensor for vegetation studies were not prioritised due to data continuity considerations. Consequently, there are several aspects of AVHRR sensor design that are not ideal for vegetation trend studies (Steven et al., 2003; Teillet et al., 1997; van Leeuwen et al., 1999), such as post-launch degradation in sensor calibrations and drift in the satellite overpass times. The seasonal variations in sun-sensor viewing geometry (as defined by the Bidirectional Reflectance Distribution Function, BRDF) combined with sensor drift over time has a large effect on time series of observed NDVI for a given location (Pinzon et al., 2005; Tucker et al., 2005). If not corrected for, historical sensor replacements – including shifts in the satellite overpass time – will influence observed NDVI trends and thereby undermine the usefulness of the dataset for long-term trend analysis. Additionally, the spectral configuration of the AVHRR sensors (number of bands, wavelengths covered and the specific band Spectral Response Functions (SRF)) does not permit an accurate atmospheric correction scheme to be applied and absorption and scattering by atmospheric components such as water vapour (Tanré et al., 1992) and aerosols (Nagol et al., 2009) are a source of error in AVHRR estimates of surface NDVI. The AVHRR channel 2 (near-infrared band) covers wavelengths in which there is considerable absorption by water vapour in the atmosphere, influencing observed NDVI (Cihlar et al., 2001; Holben, 1986). The data reduction methodology used for transforming the 1 km resolution local coverage pixels LAC AVHRR data into global coverage pixels (GAC) and finally into an 8 km resolution grid of AVHRR NDVI also has an impact on the quality of the data (James & Kalluri, 1994).

Several studies have evaluated NDVI continuity as a function of the red and near-infrared satellite band SRF's and have proposed inter-sensor translation methods amongst the different AVHRR instruments as well as the general compatibility between AVHRR instruments and newer sensors, including the Système Pour l'Observation de la Terre (SPOT) VEGETATION, the Sea-viewing Wide Field-of-view Sensor (SeaWiFS), the MODIS and the MEdium Resolution Imaging Spectrometer (MERIS) (Beck et al., 2011; Brown et al., 2006; Fensholt & Sandholt, 2005; Fensholt et al., 2006b; Pedelty et al., 2007; Swinnen & Veroustraete, 2008; Tucker et al., 2005). It remains a challenge to produce a long-term, consistent, NDVI time series across the sequence of multiple sensor systems with their different spectral responses, spatial resolutions, swath width and orbiting geometry. However, 3 global NDVI data products (Pathfinder AVHRR Land (PAL)) (James & Kalluri, 1994), the Fourier-Adjustment, Solar zenith angle corrected, Interpolated Reconstructed (FASIR) (adopted from PAL; Los et al., 2000) and NASA Global Inventory, Monitoring, and Modelling Studies (GIMMS) (Tucker et al., 2005) have been created from the spatially and temporally comprehensive AVHRR GAC dataset and are important for detection of global scale long-term trends in land degradation and vegetation productivity. Currently the NASA-funded Land Long Term Data Record (LTDR) are developing daily reflectance data from 1981 to 2000 that includes an improved atmospheric correction scheme and BRDF corrections (Pedelty et al., 2007). Two recent studies (Alcaraz-Segura et al., 2010a and Beck et al., 2011) conducted an intercomparison of these four AVHRR based NDVI dataset for the overlapping period 1982–1999 for the Iberian Peninsula and on a global scale respectively.

The only updated global coverage AVHRR dataset, covering the full period from 1981 to present, is the GIMMS. A release of the global coverage GIMMS data (1981–2006) (GIMMSg) was made available in 2007 and recently an updated GIMMS NDVI dataset (GIMMS3g; covering from 1981 to 2010) has been processed and made available by the GIMMS research group. The GIMMS correction scheme (Empirical Mode Decomposition (EMD) transformation method) (Pinzon et al., 2005) implies that the GIMMS dataset is dynamic by nature and must be re-calculated every time more recent years of data are added.

The possibilities of testing the quality and reliability of GIMMS NDVI time series trend analyses on a global scale have been limited

by the lack of an appropriate time series of data from other moderate/coarse resolution satellite sensors of adequate quality. Only since late '90s have other instruments, with improved sensor attributes like Terra MODIS, started to make NDVI time-series measurements. The processing of MODIS NDVI is based on spectral bands that are specifically designed for vegetation monitoring and include state-of-the-art navigation, atmospheric correction, reduced geometric distortions and improved radiometric sensitivity (Huete et al., 2002). MODIS NDVI is therefore considered to be an improvement over the NDVI product derived from the AVHRR sensors (Huete et al., 2002; Justice et al., 1998). With the current availability of 11 years of Terra MODIS NDVI (March 2000–present) an evaluation of the reliability of GIMMS NDVI trends for this time-span can be performed. This time period includes the operational use of four different AVHRR sensors; NOAA-14, NOAA-16, NOAA-17 and NOAA-18, each having a different Equator passing time (morning and afternoon satellites are combined) and varying degrees of orbital drift (Pinzon et al., 2007). The combined effect on the sun-sensor geometry (as expressed by the BRDF) will influence the observed NDVI if not corrected for and 2000–2010 therefore serves as a well suited period for studying the successfulness of the GIMMS NDVI correction method.

In this study the quality of the GIMMS3g NDVI data will be evaluated against MODIS NDVI using pixel wise linear regression analysis. Trend analyses of 11 years of overlapping monthly and annually integrated global scale NDVI data (2000–2010) from the two different sensor systems are intercompared on a continental scale and as a function of land cover classes. Direct per-pixel comparisons between GIMMS and MODIS NDVI are conducted and studied at the continental, regional and land cover class scale using pixel wise linear regression between Terra and Aqua MODIS NDVI (2003–2010) as a reference.

## 2. Data and methods

### 2.1. GIMMS 15-day composite NDVI product (GIMMS3g)

The series of AVHRR instruments have a 110° across-track field of view allowing for near-daily global coverage. The GIMMS NDVI dataset is based on the GAC 1B product (Goward et al., 1993). GAC data were derived by onboard averaging and sampling of the 1.1 km full resolution data LAC to a 4 km resolution (Townshend, 1994). For a given scan line the first four pixels out of five are averaged and only every third scan line is processed resulting in a nadir cell-size of 1.1 km × 4 km with a gap of 2.2 km across the scan lines (Kidwell, 1991). The channel 1 and 2 data used for the GIMMS data are calibrated as suggested by Vermote and Kaufman (1995), and the derived NDVI is further adjusted using the technique of Los (1998). The cloud detection algorithm is based on reflectance and brightness temperature values (Stowe et al., 1991; Tucker et al., 2005). No atmospheric correction is applied to the GIMMS data except for volcanic stratospheric aerosol periods (1982–1984 and 1991–1994) (Tucker et al., 2005). A satellite orbital drift correction is performed using an empirical mode decomposition/reconstruction (EMD) method of Pinzon et al. (2005) minimising effects of orbital drift by removing common trends between time series of Solar Zenith Angle (SZA) and NDVI. The GIMMS3g NDVI data is provided in 1/12-degree resolution and is processed to match the range of SPOT Vegetation and MODIS (Tucker et al., 2005) enabling the advantages of the MODIS NDVI and VGT NDVI data to be used in conjunction with the historical information provided by the GIMMS dataset. NDVI quality flags are embedded in the 15-day maximum value compositing (Holben, 1986) data files, providing information on per-pixel NDVI status identical to earlier versions of the GIMMS data. NDVI that are flagged as influenced by clouds or snow cover (flag = 1–5) are retrieved from either spline interpolation or average seasonal profiles whereas flag = 0

indicates good value and flag 6 = missing data (Pinzon et al., 2007). Only good value GIMMS NDVI pixels are included the current GIMMS-MODIS NDVI correlation analysis.

The GIMMS data used in the current analysis (2000–2010) originates from the NOAA-14 sensor (Jan. 1995 to Nov. 2000), NOAA-16 (Nov. 2000–Dec. 2003), NOAA-17 (Dec. 2003–Dec. 2008) and NOAA-18 (Jan. 2009–Dec. 2010). NOAA-14, 16 and -18 have an afternoon overpass and NOAA-17 a morning overpass. Equator crossing time for NOAA-14 afternoon satellite shifted from 13.40 in 1995 to 16.15 in 2000; NOAA-16 shifted from 14.00 in 2000 to 14.10 in 2003 (<http://nsidc.org>), NOAA-17 shifted from approximately 10.15 in 2003 to 09.45 in 2007 (Ignatov et al., 2004) and very limited drift in NOAA-18 is reported (Thorne et al., 2011). NOAA-16, 17 and 18 are carrying an AVHRR-3 type of radiometer whereas the NOAA-14 is equipped with an AVHRR-2 type of radiometer.

## 2.2. MODIS monthly composite NDVI data

The sun-synchronous orbits of Terra and Aqua MODIS cross the dayside equator at 10:30 am and 1:30 pm local crossing time, with a 16-day repeat cycle. The MODIS instrument has a 110° across-track field of view and senses the entire equator every 2 days (Wolfe et al., 1998). The MODIS NDVI 0.05-degree monthly product (MOD13C2, collection 5) is based on spatial and temporal averages of 16-day 1-kilometre NDVI (MOD13A2) (Solano et al., 2010). MOD13A2 is processed from the MODIS level 2 (L2G) daily surface reflectance product (MOD09 series) that provides red and near infrared surface reflectance corrected for the effect of atmospheric gases, thin cirrus clouds and aerosols. The MOD09 bands 1–7 product is an estimate of the surface spectral reflectance as would be measured at ground level if there were no atmospheric scattering or absorption (Vermote et al., 2002). The MOD13C2 vegetation product contains a data quality assessment (QA-data) product holding information on overall usefulness and cloud conditions on a per-pixel basis. In this work the QA screening approach suggested by Samanta et al. (2010) has been applied: For a MODIS pixel to be included in the correlation analyses the overall usefulness information must be  $\leq 11$ . The “Adjacent cloud

detected,” “Mixed clouds” and “Possible shadow” flag values must be equal to 0 and “Aerosol Quantity” flag must equal 1 (low aerosol) or 2 (average aerosol). A detailed explanation of MOD13A2 VI QA binary data may be found at ([http://lpdaac.usgs.gov/modis/qa/mod13a2\\_qa\\_v5.asp](http://lpdaac.usgs.gov/modis/qa/mod13a2_qa_v5.asp)).

## 2.3. Global land cover data

Global land cover classes (GLC-2000, Bartholomé et al., 2002) are shown in Fig. 1 and will function as a reference for further analysis and discussion of regions of MODIS/GIMMS NDVI agreement and discrepancies.

## 2.4. Data post-processing

### 2.4.1. Spatio-temporal resampling

The original GIMMS 15-day NDVI composite data covering the period from January 1982 to December 2010 were aggregated to monthly data using a maximum value composite approach to further reduce the influence from clouds. Aggregating into monthly observations also reduces the effect of sub-monthly shifts in the phenological cycle that can potentially influence the calculated trends when using standard trend estimators (where each composite is compared with the corresponding composite in other years) over too short a composite period (de Jong et al., 2011). NDVI exhibits some scale dependency since the index is a non-linear transformation and therefore the spatial resampling of the MODIS 0.05-degree resolution data should not be performed directly on the NDVI data but rather on the surface reflectance data. Terra MOD13C2 0.05-degree red and near-infrared reflectance data have therefore been resampled to match the GIMMS3g 1/12-degree resolution by spatial averaging before calculating the NDVI. As Terra was undergoing commissioning in the first two months of the year 2000, average values from the first two months of 2001–2010 are used to obtain a full year of data.

Per-pixel QA information in both the GIMMS and MODIS products allows for removal of most contamination of the NDVI signal related to clouds, aerosol and snow. To gap-fill the MODIS and GIMMS data

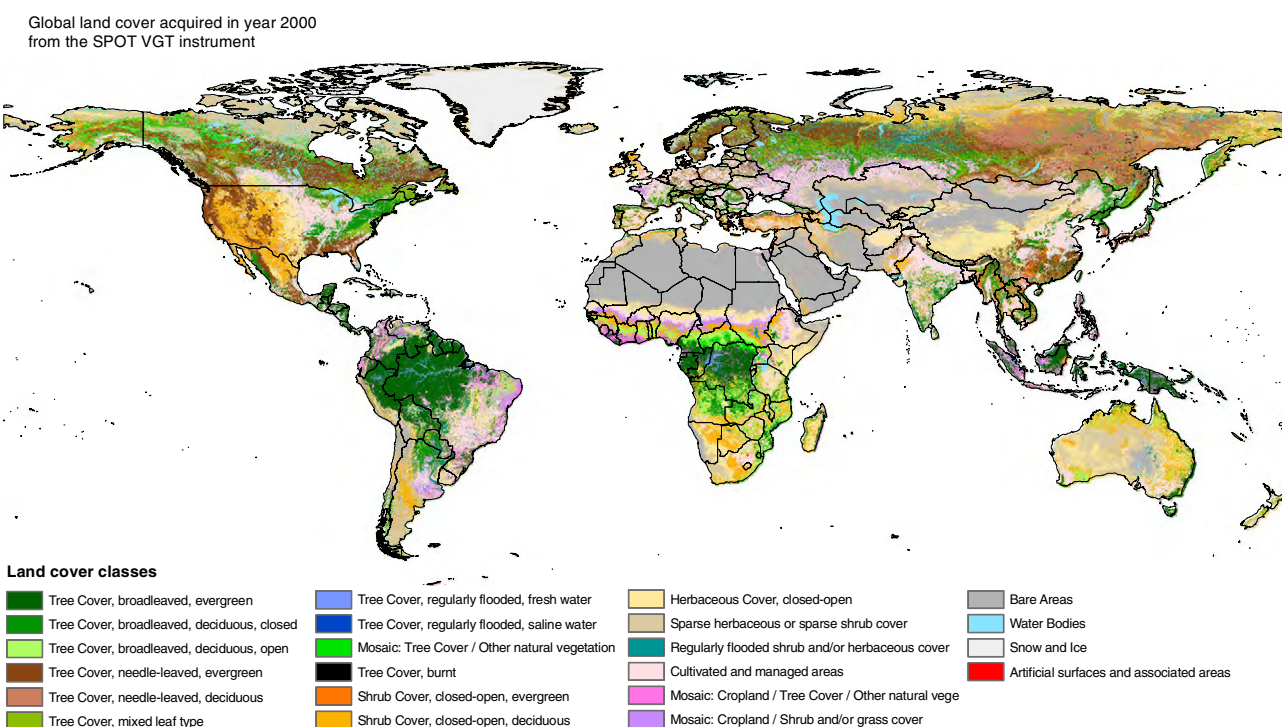


Fig. 1. Global land cover (GLC-2000) (Bartholomé et al., 2002).

prior to the trend analysis a simple temporal filter was applied to the monthly composite datasets (Fensholt et al., 2006a; Fensholt et al., 2009; Xiao et al., 2003). A time series filter including 5 composite images is applied and for a given pixel NDVI value (NDVI0) two previous (NDVI – 1, NDVI – 2) and subsequent (NDVI + 1, NDVI + 2) composite period values are considered by the following rules: If NDVI 0 is flagged as cloudy an average between NDVI – 1, NDVI + 1 is performed; if only one of NDVI – 1 or NDVI + 1 is cloud free NDVI 0 will be replaced by this value. If both NDVI – 1 and NDVI + 1 are flagged as cloudy then the filter is extended to cover also NDVI – 2 and NDVI + 2 following the same rules as for NDVI – 1 and NDVI + 1.

## 2.5. Statistical methodology

A range of statistical techniques were applied to assess the correspondence in spatio-temporal trends of the 11-year time-series of NDVI from MODIS and GIMMS and the strength of linear association between the two datasets. Temporal trends in the datasets were examined by applying a simple linear regression model with time as the independent variable and NDVI as the dependent variable. The outputs of the trend analyses are maps of correlation coefficients (*r*-values) and regression slope values, indicating the strength and magnitude of the calculated trend. Two different non-parametric statistical methods were applied in the data pre-processing according to the presence of snow cover during the period of analysis as given by the GIMMS and MODIS QA-data. Overall, pixels not influenced by snow cover during the period of analysis were studied using a test based on monthly observations whereas pixels characterised by snow cover were studied using a test based on annual integrals of the growing season (based on seasonal parameterisation of the monthly observations). This dual approach was selected to ensure that changes in the length of seasonal snow cover do not influence on the long-term NDVI trends. The trend statistics were summarised for individual continents and land cover classes. The GLC-2000 (Bartholomé et al., 2002) global land cover product was selected due to its independence of both the MODIS and AVHRR data stream.

The strength of linear association between the two datasets was determined by calculating the per-pixel Pearson product moment correlation coefficient (*r*) for the two 11-year time series of monthly observations that passed QA screening. This was done on detrended time series of data (as described by Zhou et al. (2001)) to avoid spurious regressions in the case of variables with a co-varying trend. The strength of linear association between Terra and Aqua MODIS NDVI (2003–2010) was also calculated as a reference to indicate whether discrepancies found between GIMMS and MODIS NDVI can be attributed to data processing differences or general limitations of the sensor to optical remote sensing. The regression slope statistics were binned using the GLC-2000 to study the possible impact on the relation due to differences in land cover types. Areas characterised by MODIS/GIMMS linear trend regression slopes that deviated the most from 1 were studied in greater detail. Twelve regions were selected (each covering 2000 pixels ~170,000 km<sup>2</sup>) to further analyse these major regression slope anomalies found for different mixtures of land cover classes.

### 2.5.1. Areas not influenced by snow cover

Since time-series of NDVI often do not meet parametric assumptions of normality and homoscedasticity (Hirsch & Slack, 1984) a median trend (Theil-Sen) procedure was applied. The Theil-Sen procedure is a rank-based test that calculates the non-parametric slope and intercept of the series by determining the median of all estimates of the slopes derived from all pairs of observations (Hoaglin et al., 2000). Non-parametric tests such as Theil-Sen (TS) are known to be robust against seasonality, non-normality, heteroscedasticity and temporal autocorrelation (at both intra- and inter annual scale) (Alcaraz-Segura et al., 2010b; Hirsch & Slack, 1984; Vanelle &

Hughes, 1984) and are suggested for studies of vegetation trends based on time-series of NDVI data (de Beurs & Henebry, 2005). Because of the less rigorous parametric assumptions using a non-parametric test, the TS trend analysis allows for preservation of the full temporal resolution of the NDVI data rather than analysing growing season or annually integrated values of NDVI. The TS procedure is furthermore resistant to outliers and therefore suitable for assessing the rate of change in short or noisy series (Eastman et al., 2009).

The significance of the time series trends was calculated by the non-parametric Mann-Kendall (MK) significance test. The MK significance test is commonly used as a trend test for the TS median slope operator (Eastman et al., 2009) and produce outputs of z-scores which allows for the assessment of both the significance and direction of the trend. A positive slope ( $z \geq 1.96$ ) represents a significant increase ( $\alpha = 0.05$ ) in NDVI for the period 2000–2010 and negative slopes ( $z \leq -1.96$ ) indicate a significant decrease ( $\alpha = 0.05$ ) over time.

### 2.5.2. Areas influenced by snow cover

To avoid any influence from year-to-year variations in snow cover on the calculated NDVI trends, the per-pixel growing season NDVI integral is computed from time series parameterisation using a Savitzky-Golay filter available in the TIMESAT software (Jonsson & Eklundh, 2002, 2004). The Savitzky-Golay filter is a moving filter fitting values from a least squares fit to a polynomial (Jonsson & Eklundh, 2004). The polynomial is fitted to data points within a moving window of a certain width and the width of the window affects both the degree of smoothing and the ability to follow rapid changes. The fitting is performed in several steps allowing for an adaptation to the upper envelope of the NDVI curve based on different weights assigned to data points above and below the result of the previous steps (Jonsson & Eklundh, 2004). The advantage of this approach is that the degree of adaptation to the upper envelope can be tuned to the desired level as opposed to the MVC method which always adapts to the highest NDVI values (Stisen et al., 2007). The onset and end of growing season is determined for individual years from the per-pixel polynomial fit based on a parameterisation of the fitted seasonal NDVI curve. The parameterisation is based on percentage NDVI levels of the total seasonal NDVI amplitude. The integral representing the seasonally active vegetation is estimated by the area between the fitted function and the average level of the left and right minima. The parameters applied in the TIMESAT analysis are: seasonal parameter = 0.5, Number of envelope iterations = 1, adaptation strength = 2, Savitzky-Golay window size = 2, amplitude season start and end = 30%. The trend in NDVI was then calculated from the per-pixel seasonal NDVI integrals ( $n = 11$ ) using the non parametric TS test estimating the trend regression slope and the Mann-Kendall (MK) test was used for calculating the significance of the trends.

## 3. Results

### 3.1. GIMMS and MODIS NDVI linear trends

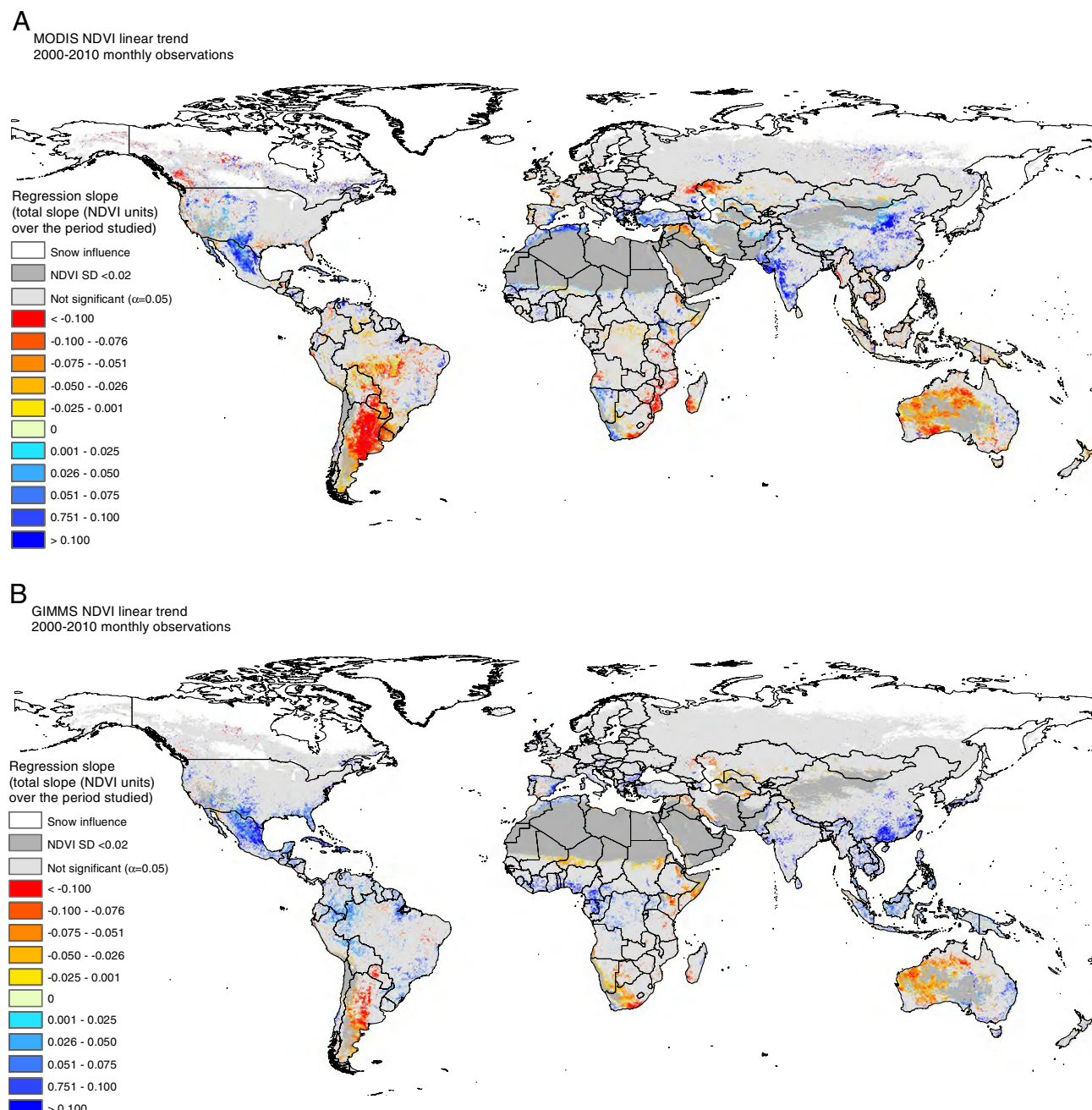
The significant trends in 2000–2010 NDVI (regression slope values) as derived from MODIS and GIMMS data are shown in Fig. 2 for areas not influenced by snow cover (assessed from the MODIS QA-data) (Fig. 2A and B) and for areas influenced by snow cover (Fig. 2C and D). Desert areas with very limited vegetation growth (here defined by an annual NDVI standard deviation (SD) of  $<0.02$ ) have been masked out because of the uncertainty related to the vegetation index estimate for such sparse vegetation cover. This threshold does not conflict with evergreen forest pixels as all were found to have  $>0.02$  annual NDVI SD. Statistics of pixels with significant positive/negative regression slopes are reported for each continent (total number of pixels and in %) in Table 1.

Scatterplots (density distribution plots) of the calculated significant trends (regression slope values) from monthly and seasonally integrated observations of MODIS and GIMMS NDVI are subdivided by continent (Fig. 3A and B) to study regression slope value consistency on a continental scale. Trend statistics of the MODIS and GIMMS NDVI analyses are calculated for the major land cover classes (GLC-2000) as presented in Table 2.

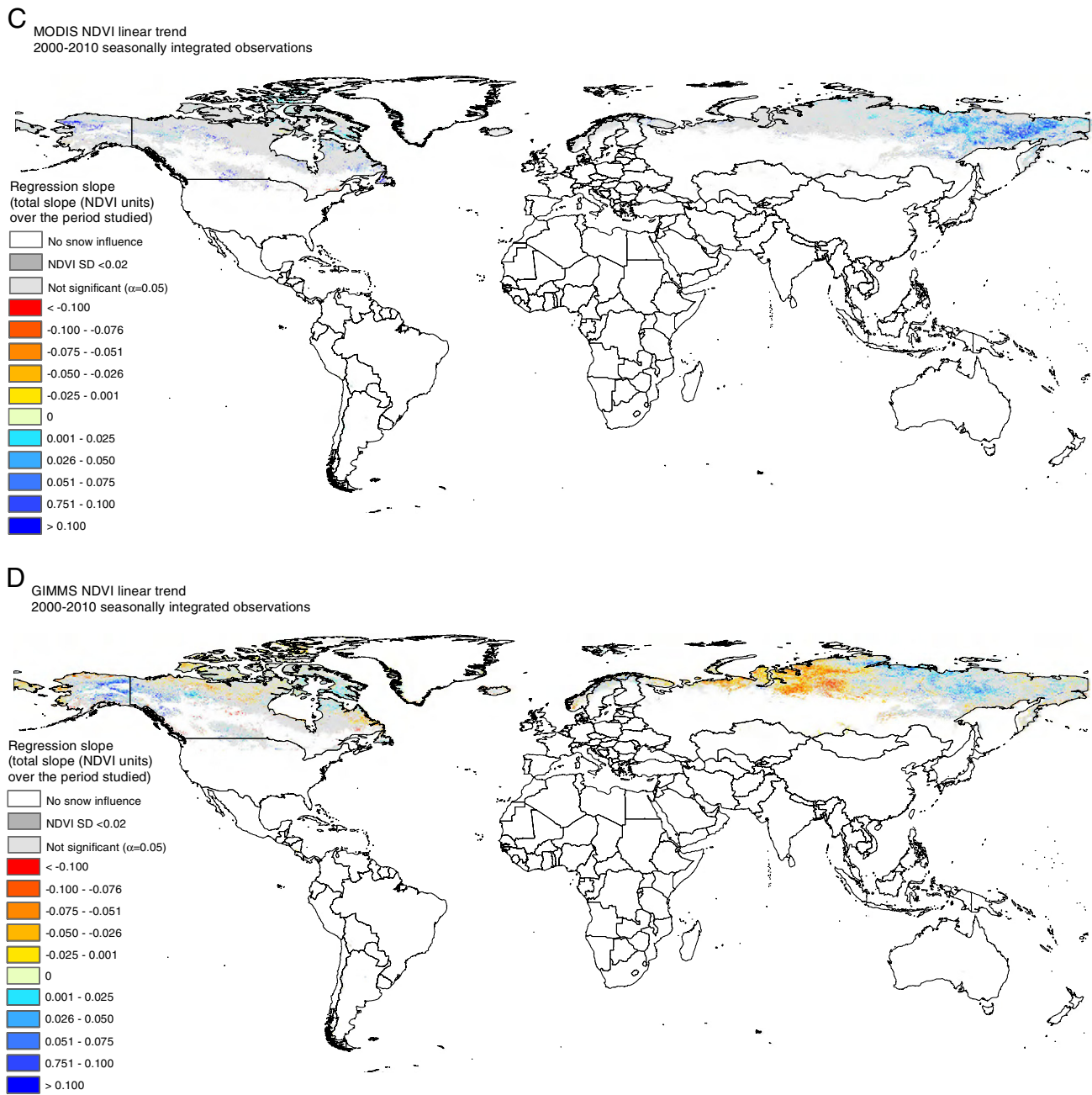
### 3.2. Direct comparison of GIMMS and MODIS NDVI

The per-pixel linear correlation between GIMMS and MODIS NDVI for monthly observations covering the period 2000–2010 and Terra/Aqua

monthly MODIS NDVI (2003–2010) are shown in Fig. 4A and B. These analyses include only observations passing the QA screening and with annual NDVI standard deviation of  $>0.02$ . No-data is assigned to pixels from which too few good pixels were available for the linear correlation analysis and only pixels significant at the 95% level are shown in colour. The corresponding regression slope values from the MODIS/GIMMS NDVI linear correlation (GIMMS NDVI being the dependent variable) and MODIS Terra and Aqua NDVI (Aqua NDVI being the dependent variable) are shown in Fig. 4C and D. The per-pixel total number of good observations (passing the QA data screening) for MODIS/GIMMS (Fig. 4A) and MODIS Terra/Aqua (Fig. 4B) are shown in Fig. 4E and F. Finally, the spatial distribution of the difference in MODIS and GIMMS NDVI mean



**Fig. 2.** (A) MODIS NDVI linear trend regression slope values (2000–2010 monthly observations for pixels not influenced by snow cover). (B) GIMMS NDVI linear trend regression slope values (2000–2010 monthly observations for pixels not influenced by snow cover). (C) MODIS NDVI linear trend regression slope values (2000–2010 seasonally integrated observations) for pixels influenced by snow cover. (D) GIMMS NDVI linear trend regression slope values (2000–2010 seasonally integrated observations) for pixels influenced by snow cover.

**Fig. 2 (continued).****Table 1**

Trend statistics for MODIS and GIMMS NDVI linear trend analysis 2000–2010 ( $\alpha = 0.05$ ). For North America and Asia pixel statistics from both snow cover influenced areas and areas without snow influence are combined.

| Number of observations                    | North America | South America | Europe  | Africa  | Asia    | Australia | All continents |
|---|---------------|---------------|---------|---------|---------|-----------|----------------|
| Total pixels (n) excluding NDVI SD < 0.02 | 460,698       | 208,905       | 206,290 | 240,547 | 683,330 | 79,830    | 1,879,600      |
| MOD13 NDVI positive regression slope (n)  | 25,439        | 6252          | 1140    | 12,747  | 53,967  | 2386      | 101,931        |
| MOD13 NDVI negative regression slope (n)  | 6412          | 51,986        | 2977    | 15,497  | 15,865  | 26,583    | 119,320        |
| MOD13 NDVI positive regression slope (%)  | 5.5           | 3.0           | 0.6     | 5.3     | 7.9     | 3.0       | 5.4            |
| MOD13 NDVI negative regression slope (%)  | 1.4           | 24.9          | 1.4     | 6.4     | 2.3     | 33.3      | 6.3            |
| GIMMS NDVI positive regression slope (n)  | 24,967        | 18,685        | 1092    | 10,693  | 32,320  | 3521      | 91,278         |
| GIMMS NDVI negative regression slope (n)  | 15,665        | 13,357        | 738     | 15,006  | 42,599  | 17,871    | 105,236        |
| GIMMS NDVI positive regression slope (%)  | 5.4           | 8.9           | 0.5     | 4.4     | 4.7     | 4.4       | 4.9            |
| GIMMS NDVI negative regression slope (%)  | 3.4           | 6.4           | 0.4     | 6.2     | 6.2     | 22.2      | 5.6            |

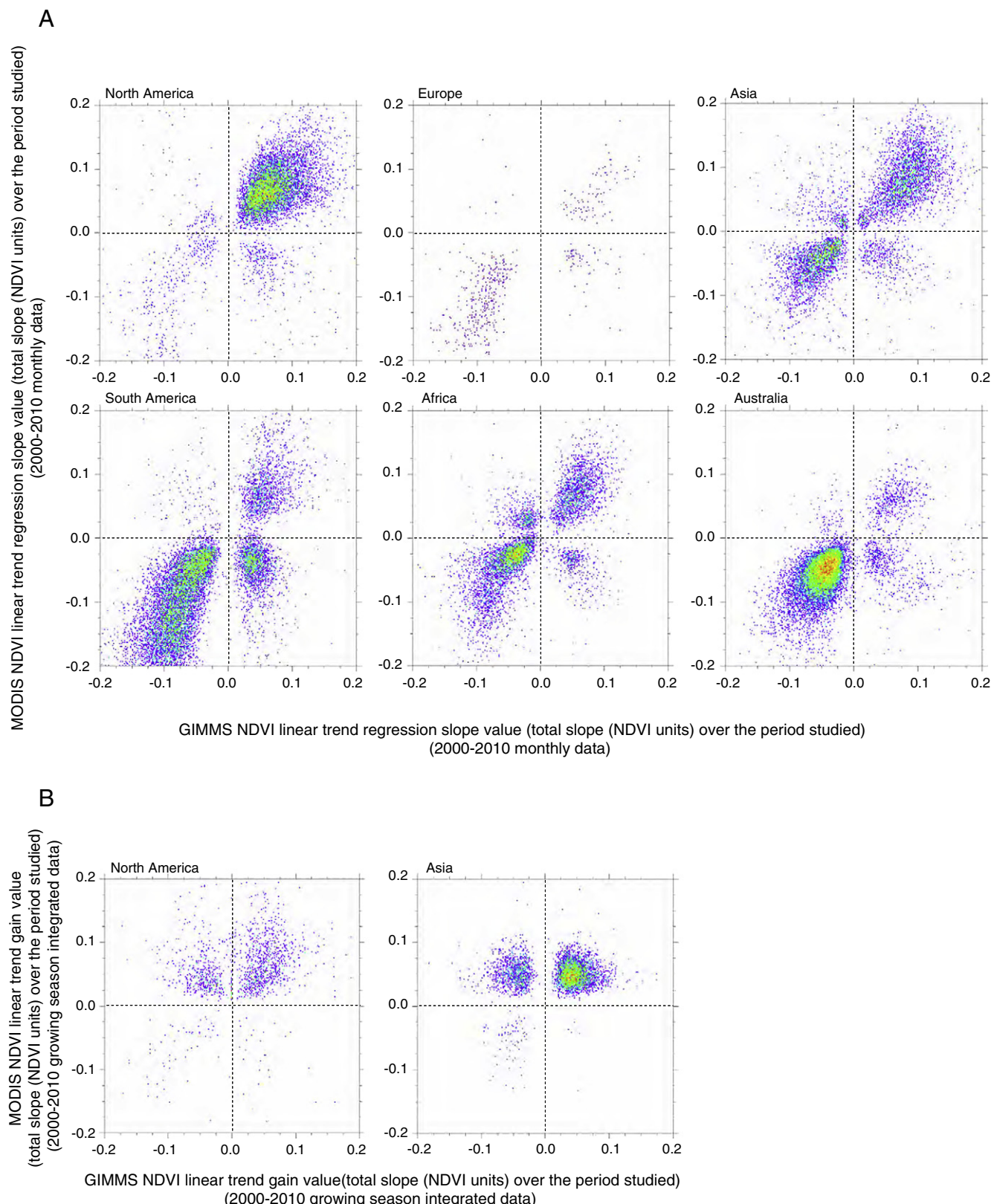


**Fig. 3.** (A) Density scatterplot (per continent) of GIMMS NDVI linear trend regression slope values (2000–2010 monthly data;  $\alpha = 0.05$ ) against MODIS NDVI linear trend regression slope value (2000–2010 monthly data;  $\alpha = 0.05$ ) for pixels not influenced by snow cover. (B) Density scatterplot (per continent) of GIMMS NDVI linear trend regression slope values (2000–2010 seasonally integrated observations;  $\alpha = 0.05$ ) against MODIS NDVI linear trend regression slope value (2000–2010 seasonally integrated observations;  $\alpha = 0.05$ ) for pixels influenced by snow cover.

annual SD are calculated (Fig. 4G) and the observed MODIS and GIMMS NDVI differences for selected regions are discussed (regions of further analysis are superimposed).

The GIMMS/MODIS significant linear trend regression slope values (GIMMS NDVI being the dependent variable) are plotted against the GIMMS/MODIS r values as density plots on a continental scale in Fig. 5.

**Table 2**

Trend statistics for MODIS and GIMMS NDVI linear trend analysis 2000–2010 ( $\alpha = 0.05$ ) for major land cover classes (GLC 2000).

| Land cover class (GLC 2000)                          | GIMMS n<br>( $\alpha = 0.05$ ) | GIMMS<br>slope > 0 (%) | GIMMS<br>slope < 0 (%) | GIMMS regression<br>slope value mean | MODIS n<br>( $\alpha = 0.05$ ) | MODIS<br>slope > 0 (%) | MODIS<br>slope < 0 (%) | MODIS regression<br>slope value mean |
|--|--------------------------------|------------------------|------------------------|--------------------------------------|--------------------------------|------------------------|------------------------|--------------------------------------|
| Tree cover, broadleaved, evergreen                   | 28,106                         | 91.2                   | 8.8                    | 0.045                                | 28,132                         | 14.6                   | 85.4                   | -0.037                               |
| Tree cover, broadleaved, deciduous, closed           | 4782                           | 65.3                   | 34.7                   | 0.023                                | 10,250                         | 23.2                   | 76.8                   | -0.053                               |
| Tree cover, broadleaved, deciduous, open             | 3765                           | 52.6                   | 47.4                   | 0.002                                | 5660                           | 12.9                   | 87.1                   | -0.068                               |
| Tree cover, needle-leaved, evergreen                 | 15,723                         | 75.6                   | 24.4                   | 0.042                                | 15,149                         | 52.8                   | 47.2                   | -0.009                               |
| Tree cover, needle-leaved, deciduous                 | 11,009                         | 48.1                   | 51.9                   | -0.002                               | 13,168                         | 97.4                   | 2.6                    | 0.060                                |
| Tree cover, mixed leaf type                          | 2130                           | 68.7                   | 31.3                   | 0.036                                | 2112                           | 53.7                   | 46.3                   | 0.022                                |
| Mosaic: Tree cover/other natural vegetation          | 8421                           | 69.5                   | 30.5                   | 0.027                                | 4956                           | 82.5                   | 17.5                   | 0.054                                |
| Shrub cover, closed-open, evergreen                  | 6109                           | 78.9                   | 21.1                   | 0.047                                | 5164                           | 73.4                   | 26.6                   | 0.033                                |
| Shrub cover, closed-open, deciduous                  | 36,199                         | 38.8                   | 61.2                   | -0.011                               | 35,890                         | 59.7                   | 40.3                   | 0.009                                |
| Herbaceous cover, closed-open                        | 31,386                         | 32.7                   | 67.3                   | -0.012                               | 37,274                         | 48.5                   | 51.5                   | 0.003                                |
| Sparse herbaceous or sparse shrub cover              | 51,024                         | 27.7                   | 72.3                   | -0.020                               | 44,135                         | 39.5                   | 60.5                   | -0.014                               |
| Regularly flooded shrub and/or herbaceous cover      | 4812                           | 34.4                   | 65.6                   | -0.018                               | 4144                           | 38.7                   | 61.3                   | -0.018                               |
| Cultivated and managed areas                         | 17,327                         | 75.9                   | 24.2                   | 0.043                                | 29,886                         | 58.7                   | 41.3                   | 0.013                                |
| Mosaic: Cropland/tree cover/other natural vegetation | 6586                           | 90.9                   | 9.1                    | 0.050                                | 7886                           | 18.4                   | 81.6                   | -0.041                               |
| Mosaic: Cropland/shrub and/or grass cover            | 2559                           | 39.7                   | 60.3                   | -0.021                               | 5674                           | 27.1                   | 72.9                   | -0.049                               |

Areas characterised by MODIS/GIMMS regression slope values that deviate the most from 1 are generally coincident with areas with the largest deviation in MODIS and GIMMS NDVI annual SD (Fig. 4G). Monthly NDVI (average of 2000 pixels) from MODIS and GIMMS (2000–2010) are shown as time series and scatterplots in Fig. 6A and B for 12 selected locations (locations superimposed in Fig. 4G). The trend regression slope value statistics calculated per land cover class for pixels with a strong association between MODIS and GIMMS monthly NDVI ( $p < 0.01$ ) are provided in Table 3.

## 4. Discussion

### 4.1. GIMMS and MODIS NDVI linear trends

A mixed pattern of areas of increasing and decreasing greenness can be observed from both the GIMMS and MODIS NDVI datasets (Fig. 2) and the number of pixels with a significant NDVI trend for all continents in total is fairly similar for MODIS and GIMMS (Table 1). A significant trend in NDVI was found for 11.8% of the MODIS pixels on a global scale (excluding areas of NDVI SD  $< 0.02$ ) (5.4% having positive trends and 6.3% of negative trends) whereas the GIMMS NDVI analysis produced a total of 10.5% significant pixels (4.9% positive and 5.6% negative).

#### 4.1.1. Areas of negative NDVI trends

Both datasets generally show large areas of significant negative trends in Argentina, Australia, south eastern part of southern Africa, and for some smaller areas in East Africa (Ethiopia, Somalia, Kenya and Tanzania), Middle East (stretching from Syria to Iran), the border area between Russia and Western Kazakhstan and south western Canada. On a continental scale the areas of significant NDVI change are in good agreement for North America, Europe, Africa and Asia (Table 1). There are, however, larger differences in the results from South America and Australia with differences of 12.5% and 9.5% respectively. The larger difference in the magnitude and direction of trends is especially pronounced for South America where pixels with a significant negative regression slope from the MODIS analysis cover 24.9% of the continent but only 6.4% from the GIMMS based analysis. The regions of significantly decreased NDVI, as observed from GIMMS trends, cover primarily Argentina and Paraguay. The MODIS data shows decreasing trends extending further North and West, covering a larger part of the South American continent including Uruguay, parts of Bolivia and the Amazonian basin (Rondonia and Matto Grosso). The magnitude of negative change is also generally larger in the MODIS data for South America as compared to the GIMMS derived regression slope values. For Australia there is a predominant negative trend from both datasets and a general agreement

in the magnitude of decreasing trends in NDVI. However, statistics (Table 1) show that more pixels from MODIS have negative trends (33.3%) as compared to the GIMMS based analysis (22.4%). For the remaining areas mentioned, the magnitude of the negative regression slope values is similar for MODIS and GIMMS, with a tendency for larger clusters of areas being significantly negative in the analysis based on MODIS data (e.g. Mozambique and south western Canada) as compared to the more scattered appearance of GIMMS pixels.

#### 4.1.2. Areas of positive NDVI trends

Analyses from MODIS and GIMMS both indicate areas of greening in the central-north Mexico stretching into USA (Texas, New Mexico). In South America the regions bordering the Amazonian basin generally show scattered positive trends in NDVI from GIMMS whereas these areas show a more mixed pattern of positive/negative trends as calculated from MODIS data. The regions neighbouring the Mediterranean Sea have generally become greener as indicated by analyses from both datasets. The trend agreement is also noticeable in larger areas of India and China; however the spatial pattern of which specific regions pass the threshold of being significantly positive varies somewhat. The majority of the GIMMS pixels with a significant trend scattered in Equatorial Africa and South East Asia show a greening trend whereas the pattern from MODIS indicates mixed positive/negative trends. For Northern Hemisphere areas influenced by snow cover (Fig. 2C and D) (statistical trends calculated from growing season NDVI integrals) the vast majority of pixels characterised by a significant trend from MODIS data indicates a greening trend (primarily North East Siberia and scattered areas in Canada and Alaska). The GIMMS based analysis for snow covered areas on the other hand also show large areas of significantly negative trends in greenness (central and northwest Siberia) and scattered areas in coastal regions of Alaska and Canada (Labrador and Nunavut). These areas of significant negative trends coincide with areas where the MODIS trends are also generally negative, however not significant at the 95% level and therefore displayed in grey. The approach based on seasonal NDVI integrals for these high latitude areas is considered robust since these areas have a distinct unimodal growing season. Seasonality parameters (start and end of growing season) used for the seasonal integrals were derived from both the thresholds of absolute NDVI values and as a percentage of the seasonal NDVI amplitude to test the sensitivity of the different methods. The outputs of linear trend analyses from the two different approaches (absolute NDVI values/NDVI amplitude) were very similar (the results based on the percentage of the seasonal NDVI amplitude are shown). It should be noted that only 11 observations (seasonal integrals) are included making the statistical trend analysis more sensitive to the fluctuations of individual seasonal NDVI integrals even though the non parametric TS trend estimate is

found to be robust when applied on short and noisy time series data (Eastman et al., 2009). The trend for areas influenced by snow was also calculated on monthly data to assess the potential error of including winter observations (handled differently in the two datasets). However, the significant trends for monthly GIMMS and MODIS NDVI were found to be very similar to the trends based on growing season integrals.

#### 4.2. GIMMS and MODIS NDVI trend comparison

For pixels with good agreement between the NDVI trends derived from the two dataset data points in the Fig. 3A and B scatter-plots (significant regression slope values from observations of MODIS and

GIMMS NDVI) should be located in the first and third quadrants. Generally there is a good correspondence between the monthly based MODIS and GIMMS significant NDVI trend (regression slope) values for all continents (Europe having only few significant pixels though). For North America and Australia there is a good agreement between NDVI regression slope values (following the diagonal crossing the 1 and 3 quadrant) with distinct different trends; North America showing mostly positive trends (1 quadrant) and Australia showing primarily negative trends (3 quadrant). For Africa and Asia the magnitude of NDVI trend is mixed, but for the majority of pixels the sign of regression slope values is similar for the two datasets with the bulk of pixels being located in quadrants 1 and 3. For South America there is an overall agreement between the products showing a

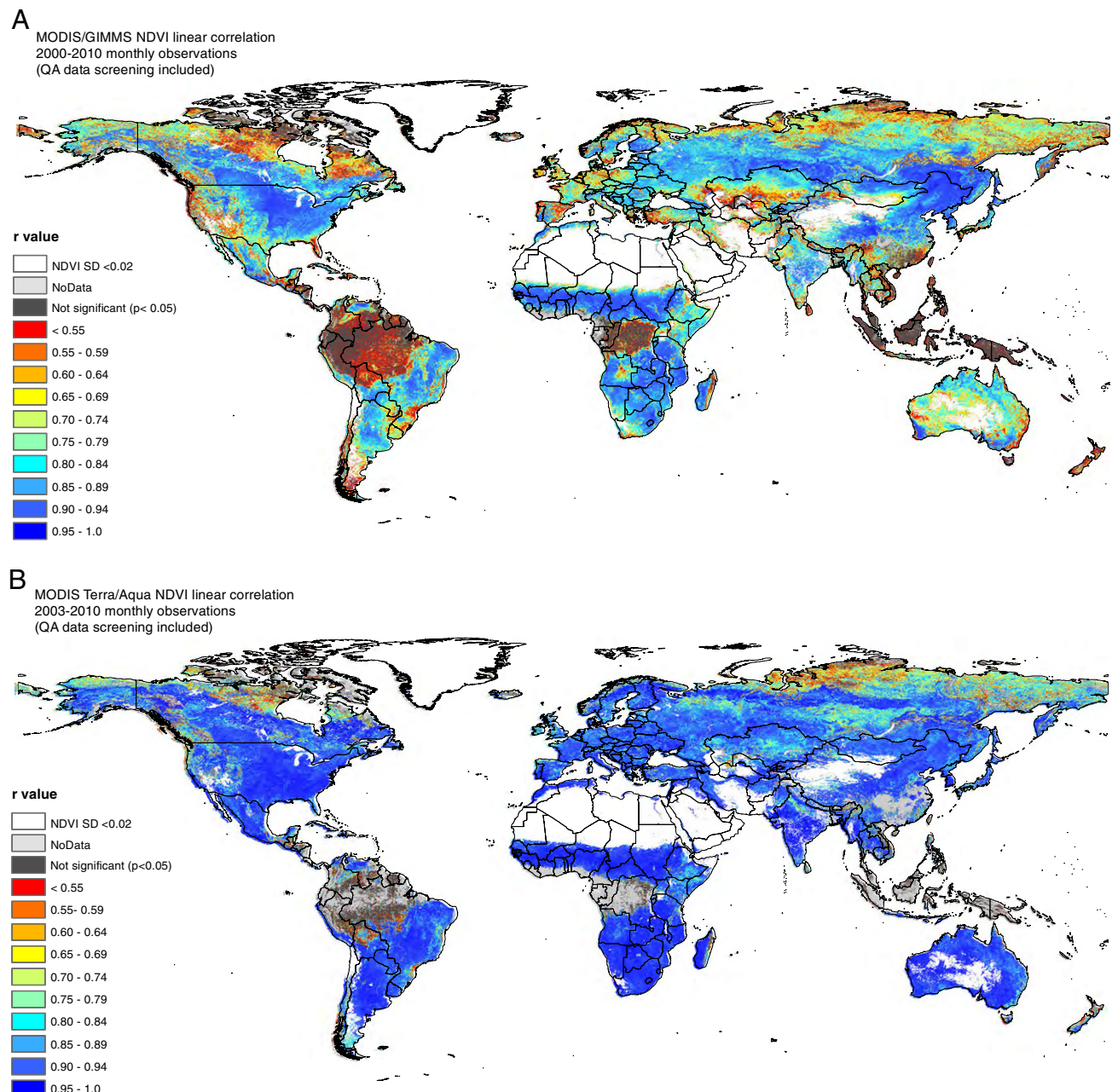


**Fig. 4.** (A) r-values from linear regression trend analysis of monthly observations of GIMMS and MODIS NDVI (2000–2010). (B) r-values from linear regression trend analysis of monthly observations of MODIS Terra and Aqua NDVI (2003–2010). (C) Regression coefficient (regression slope values) from linear regression trend analysis of monthly observations of GIMMS and MODIS NDVI (2000–2010). (D) Regression coefficient (regression slope values) from linear regression trend analysis of monthly observations of MODIS Terra and Aqua NDVI (2003–2010). (E) Total number of good observations (passing the QA screening) for MODIS/GIMMS NDVI correlation (monthly observations). (F) Total number of good observations (passing the QA screening) for MODIS Terra/Aqua NDVI correlation (monthly observations). (G) Annual standard deviation difference between MODIS and GIMMS NDVI (mean of 2000–2010 monthly observations). Regions of further analysis are superimposed.

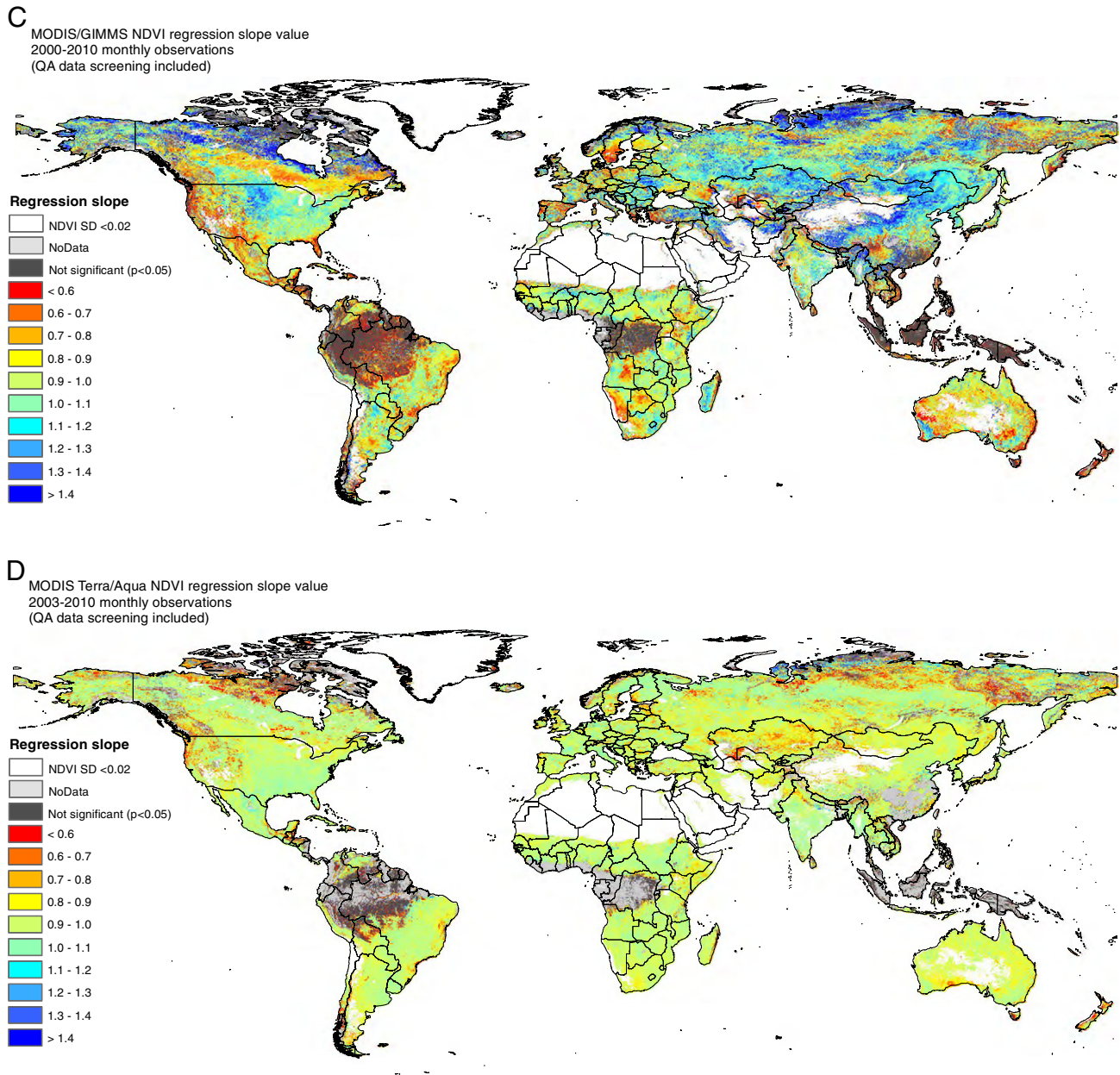


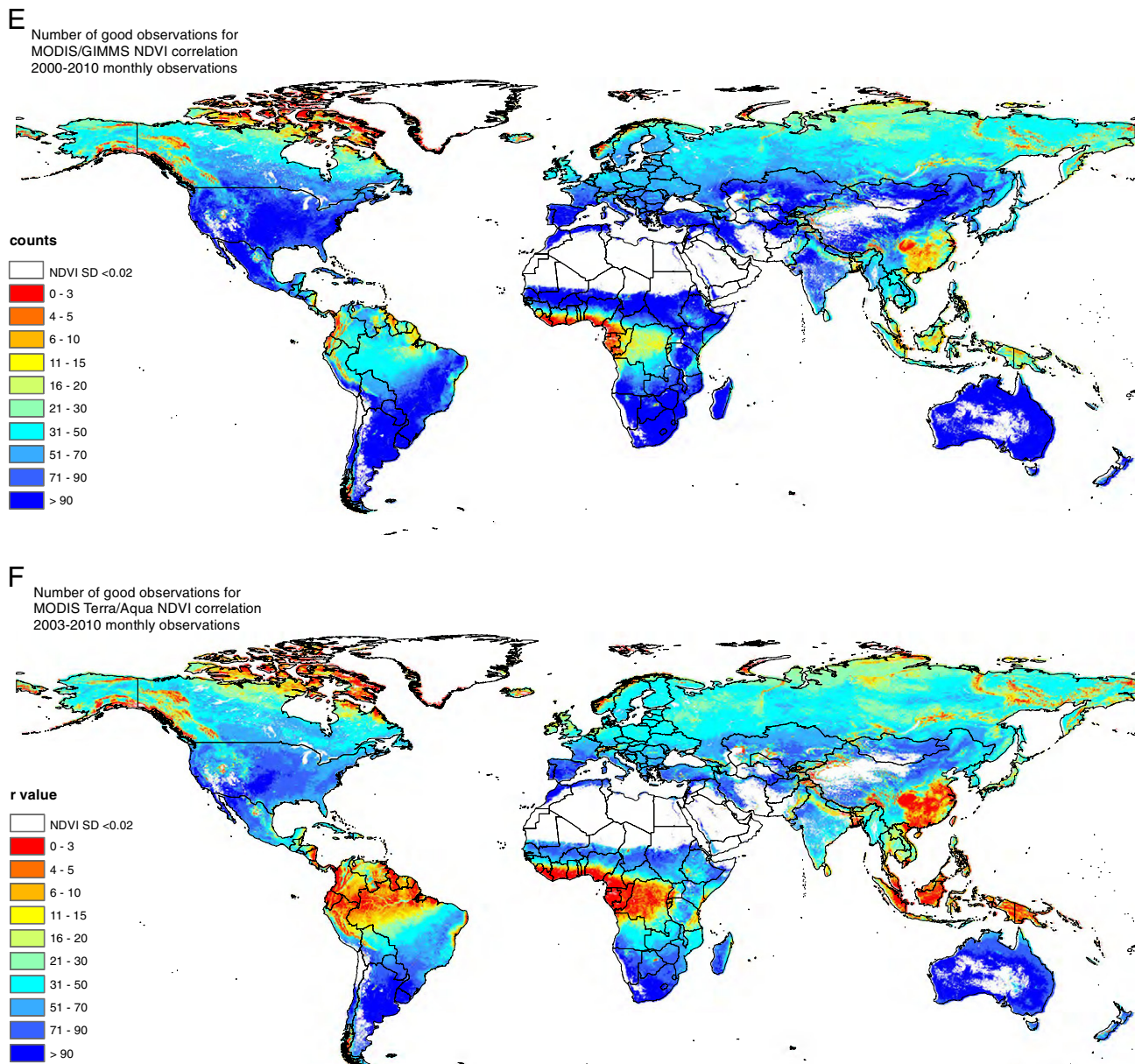
Fig. 4 (continued).

negative NDVI trend. However, for areas of large negative regression slope values MODIS generally shows stronger negative trends as compared to GIMMS. Also a large cluster of pixels of positive GIMMS regression slope values and negative MODIS regression slope values can be observed in quadrant 2. This cluster of pixels coincides primarily with the Fig. 2A and B discrepancies between MODIS and GIMMS NDVI trends in the area covering southern Brazil, Paraguay and Bolivia. For continents with pixels influenced by snow cover (North America and Asia, Fig. 3B) the significant trends in NDVI based on growing season integrated NDVI is shown. Very few pixels in Europe that are influenced by snow cover and retain a significant trend exist and therefore a scatter plot is not included. Almost all significant MODIS NDVI trends from both North America and Asia are found to indicate a greening trend over the 11 years (as also visible in Fig. 2C). The regression slope values correspond reasonably with the GIMMS based significant trends for the majority of pixels in Asia; but a bulk of pixels is located in quadrant 4 having significant positive

MODIS regression slope values and negative GIMMS values (central and northwest Siberia in Fig. 3B). This tendency is the same for North America, with larger range in the regression slope values and less significant pixels in the scatter plot. As can be seen from the land use class regression slope averages (Table 2) the agreement between trends from MODIS and GIMMS NDVI is not evident indicating that the overall agreement found between regional/continental scale patterns cannot be extended to global land cover classes.

#### 4.3. Direct comparison of GIMMS and MODIS NDVI

In general high per-pixel correlations exist between the two datasets (Fig. 4A) that indicate an equal ability of capturing the phenological growth cycle. The exception from this is the equatorial rainforest areas (Fig. 1; Tree Cover, broadleaved, evergreen) where the r values drop considerably with many scattered pixels not being significant. The lower r values are partly caused by the low annual NDVI SD for

**Fig. 4 (continued).**

rainfall forest areas producing a small range in per-pixel correlations. NDVI is also known to saturate for dense vegetation due to the strong absorption in the red band (Huete et al., 1997) which might influence the correlation and finally residual clouds might introduce noise despite the MODIS QC filtering applied. The correlation analysis conducted for Terra/Aqua monthly MODIS NDVI (Fig. 4B) also shows much lower correlations for the class of broadleaved evergreen forest. Larger areas of no-data are present in the Terra/Aqua MODIS analysis as compared to the MODIS/GIMMS analysis indicating the severe problems of cloud cover and aerosols for the majority of the equatorial rainforest areas. For the remaining equatorial rainforest areas (where number of observations supports an r-value to be calculated), Fig. 4A and B indicate an almost similar spatial extent of pixels found to have an insignificant relation between NDVI time-series. The number of observations available (Fig. 4E and F) for the calculations of Fig. 4A and B underlines the fundamental problem of studying equatorial rainforest using optical EO-systems as also discussed in Saleska et al., 2007; Brando et al., 2010 and Samanta et al., 2010.

Areas of sparse vegetation cover (Fig. 1; “Sparse herbaceous or sparse shrub cover” (primarily arctic regions) and “Herbaceous Cover, closed-open” (primarily dryland areas)) generally also show lower r values in Fig. 4A (MODIS/GIMMS NDVI). The discrepancy between GIMMS and MODIS NDVI for very high northern latitudes was also found in Beck and Goetz (2011) based on the GIMMSg. This pattern is also found to be the case for “Sparse herbaceous or sparse shrub cover” of the arctic regions in Fig. 4B based on Terra/Aqua MODIS NDVI, but not for Fig. 4B “Herbaceous Cover, closed-open” dominating in global dryland areas. This difference can be explained by the region specific number of good observations available for the correlation analyses (Fig. 4E and F). The arctic areas are constrained by the total number pixels of good observation, as was the case for the equatorial rainforest, and it is likely that some of the remaining pixels after QA screening are still influenced by clouds – thereby lowering the obtained r value. On the contrary the discrepancy between MODIS and GIMMS NDVI for the land cover class “Herbaceous Cover, closed-open” found primarily in global dryland areas is not

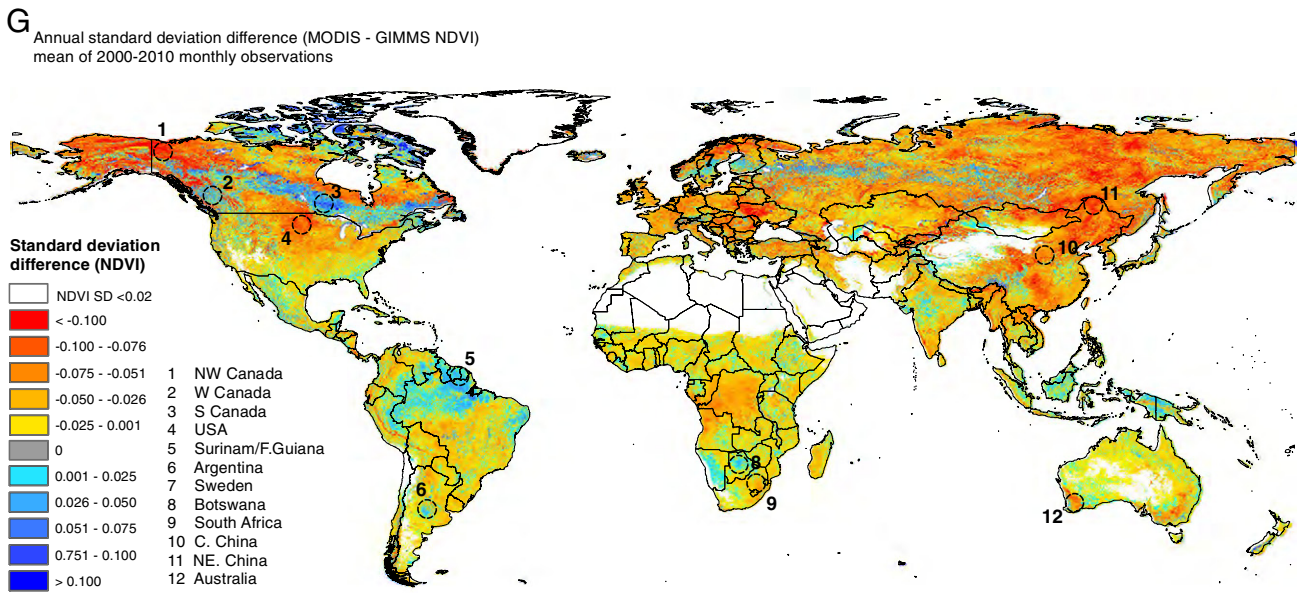


Fig. 4 (continued).

likely to be caused by the number of good observations. Close to the maximum possible number of good observations is available from both GIMMS and MODIS for these dry environments. The lower MODIS/GIMMS r values compared to Terra/Aqua MODIS therefore indicates some uncertainty related to the GIMMS NDVI estimate for areas of very limited chlorophyll activity.

Regression slope values from the MODIS/GIMMS NDVI linear correlation (GIMMS NDVI being the dependent variable) (Fig. 4C) are considerably lower than 1 for the areas of low r values (Fig. 4A) in the equatorial rainfall forest areas. For areas of high r values the regression slope between GIMMS and MODIS is expected to be more constant with a mean value close to 1. Slope values are found predominantly within the interval of 0.8–1.2 but also larger variations in the regression slope can be observed for areas of high r values like in Canada where a noticeable belt of pixels with low regression slope values crosses the country. Canada is characterised by both high r values and a high range in annual NDVI and is therefore not expected to be an area having regression slope values that deviate considerably from 1. The belt of low regression slope values however coincides with the presence of land cover class “needle-leaved evergreen forest” (Fig. 1) and the presence of “needle-leaved evergreen forest” matches the lower slope values in areas Western Canada, USA and southern Scandinavia. Also areas of high regression slope values are observed in central USA, North-western Canada and large areas in central/eastern China and Inner Mongolia. These areas coincide with the land cover classes of “Sparse herbaceous or sparse shrub cover” in North America and “Herbaceous Cover, closed-open” in Asia. The spatial differences in regression slope values also become evident from the spatial distribution of the difference in MODIS and GIMMS NDVI mean annual SD (Fig. 4G). The large positive differences in the MODIS and AVHRR GIMMS annual SD (MODIS having higher SD than GIMMS NDVI) correspond to the areas of low regression slope values in Fig. 4C and the band of SD differences visible in North America and southern Scandinavia matches the brown coloured “needle-leaved evergreen forest” in Fig. 1.

When plotting the GIMMS/MODIS significant linear regression slope values against the GIMMS/MODIS r values on a continental scale (Fig. 5) it becomes clear that the majority of pixels with a high correlation between MODIS and GIMMS NDVI also have a slope value close to 1. This is especially clear from the North American

continent and Asia having a large bulk of pixels with high r values. The density plot for North America shows a skewness for high r values towards lower regression slope values that is caused by the belt of pixels coinciding with “needle-leaved evergreen forest” as discussed above. Interestingly, for the density plot of the African continent, also with a large bulk of pixels with high r values, the regression slope values are generally lower than 1 with maximum concentrations of regression slope values around 0.9. The same tendency can be observed for pixels covering South America. Fewer pixels, however, have high r values for South America and Australia (in percentage of total pixels). The reason for the lower relative number of pixels of high MODIS/GIMMS NDVI r values in South America and Australia could in part be the lower level of seasonal dynamics in NDVI as compared to the northern hemisphere continents.

#### 4.4. Comparison of GIMMS and MODIS NDVI for selected areas

The time series and scatterplots of the regions 1–4 (Fig. 6A and B) represent areas in North America with high negative and positive slope value deviations from 1 and large differences in the annual standard deviation of MODIS and GIMMS NDVI. Regions 2 and 3 are both classified as “Tree cover, needle-leaved, evergreen” (Fig. 1) whereas region 1 is a mix of “Mosaic: Tree Cover/Other natural vegetation”, “Sparse herbaceous or sparse shrub cover” and “Shrub Cover, closed-open, deciduous” and region 4 is primarily “Cultivated and managed areas” and “Herbaceous Cover, closed-open”. GIMMS NDVI is found to be higher at the peak of the growing season than MODIS NDVI for all 4 regions (Fig. 6A 1–4). The base level of GIMMS NDVI is, however, considerably higher than MODIS NDVI for the two needle-leaved forested sites (Fig. 6A 2–3) as compared to the sites primarily classified as non-forest vegetation. The large difference in base level NDVI causes the regression slope to vary accordingly (1.10 and 1.20 in Fig. 6A 1, 4 and 0.83 and 0.73 in Fig. 6A 2–3). The bias in base level seasonal NDVI towards higher GIMMS values can be found in other regions in North America classified as “Tree cover, needle-leaved, evergreen”. Also, region 7 in Sweden (classified as “Tree cover, needle-leaved, evergreen”) has a similar NDVI seasonal distribution (Fig. 6A 7) and scatterplot (Fig. 6B 7) to region 2 and 3. Region 5 is classified as land “Tree Cover, broadleaved, evergreen” and as for larger parts of the northern Amazon (Fig. 4G) the MODIS NDVI seasonal

range is moderately higher than for GIMMS NDVI (Fig. 6B 5). GIMMS NDVI is higher than MODIS NDVI in absolute values, but the smaller range in GIMMS NDVI causes a regression slope value below 1. It should be noted that the  $r$  value is much higher from an average of 2000 pixels than in the pixel-wise correlations reported in Fig. 4A because the noise introduced from cloud cover influence in this region tends to be reduced by the spatial averaging. Region 6 is in the centre of the large South American region and shows a decreasing NDVI trend from both MODIS and GIMMS (Fig. 2A and B). The land cover of region 6 is a mix of "Cultivated and managed areas" and "Mosaic: Cropland/Shrub and/or grass cover". Here GIMMS NDVI is generally higher than MODIS NDVI – particularly in the dry season – resulting in a regression slope value of  $<1$ . For region 8 in Botswana (land cover "Shrub Cover, closed-open, deciduous" and "Herbaceous Cover, closed-open") there is a good agreement between the level of MODIS and GIMMS NDVI; however MODIS values are higher during the peak growing season thereby causing the regression slope value of  $<1$ . The land cover of region 9 (north eastern South Africa) is similar to the region 4 in central USA. Despite the smaller seasonal range of NDVI in South Africa the MODIS/GIMMS differences are similar to region 4 with GIMMS NDVI generally being higher than MODIS, with an increasing difference for larger NDVI values causing a regression slope value of  $>1$ . Similar patterns can be observed from region 12 (south-western Australia) which is a region dominated by cultivation (land cover class "Cultivated and managed areas"). Region 10 is classified as "Herbaceous Cover, closed-open" and shows a moderate range in NDVI and a larger seasonal range in GIMMS NDVI than in MODIS. This combination causes the regression slope value to be considerably higher than 1 (1.39), something

typical for large parts of China (Fig. 4B) that are classified as land cover class "Herbaceous Cover, closed-open" (Fig. 1). The land cover of region 11 that borders China and Russia is primarily "Tree Cover, needle-leaved, deciduous" and the selected region is representative of a large part of central-eastern Russia with the same land cover class, trend regression slope values moderately above 1 and negative MODIS/GIMMS SD difference. The NDVI time series and scatterplot (Fig. 6A and B 11) show that GIMMS NDVI is higher than MODIS for the peak growing season, whereas NDVI agrees better for lower values with a tendency of higher MODIS NDVI during green-up and dry down.

#### 4.5. Influence of land cover classes on GIMMS and MODIS NDVI trends

The observed regions of GIMMS/MODIS trend regression slope values that deviate the most from 1 can be seen to coincide with specific land cover classes. Hence, different types of vegetation structure appear to have an impact on the linear association between GIMMS and MODIS NDVI. GIMMS NDVI has been processed to match the range of MODIS NDVI based upon ancillary data including the IGBP land cover classification (Pinzon et al., 2007) but residual effects from varying vegetation structure inherited from land cover classes appear to remain in the GIMMS NDVI. Also Alcaraz-Segura et al. (2010b) found differences in GIMMS NDVI trends for different biomes in central Canada as compared to a 1 km AVHRR based dataset (developed by the Canadian Centre for Remote Sensing) and discussed a possible SZA drift "overcorrection" by the EMD for certain biomes. From the selected regions it is clear that largest regression slope differences are observed for "Tree cover, needle-leaved, evergreen" on the one hand (low regression slope values) and "Herbaceous Cover,

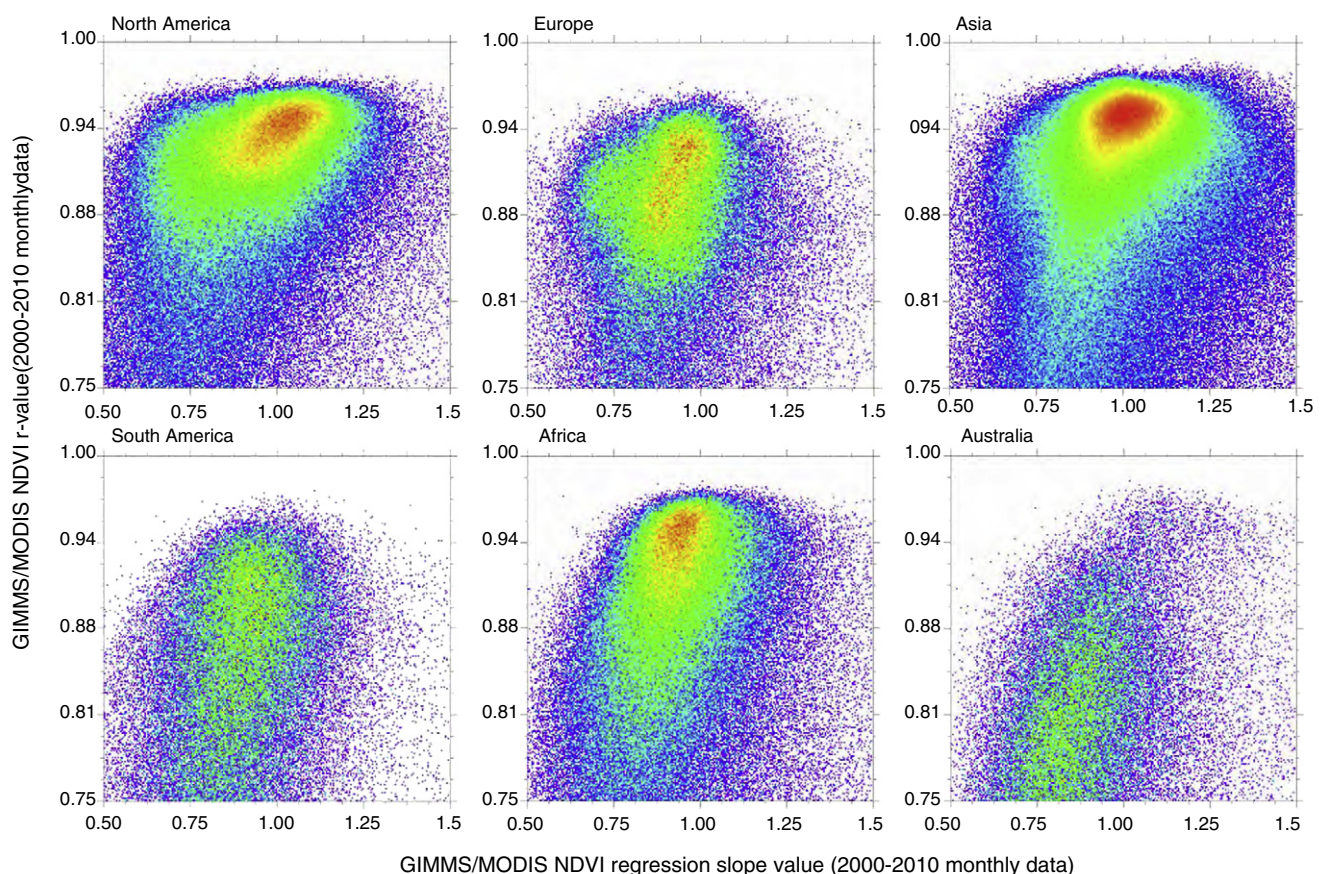


**Fig. 5.** Density scatterplot (per continent) of regression slope values from linear regression trend analysis of monthly observations of GIMMS and MODIS NDVI (2000–2010) against  $r$ -values from linear regression trend analysis of monthly observations of GIMMS and MODIS NDVI (2000–2010).

closed-open", "Sparse herbaceous or sparse shrub cover", "Cultivated and managed areas" and "Tree Cover, needle-leaved, deciduous" on the other hand (high regression slope values).

The pattern of regression slope anomalies from the selected regions (Fig. 6B) is also reflected in the global cover statistics (Table 3) (with, however, regression slope value deviations from 1 being substantially reduced by averaging over entire classes). Land cover class "Sparse herbaceous or sparse shrub cover" has the highest regression slope (1.11) followed by "Shrub Cover, closed-open, evergreen" (1.06), "Tree Cover, needle-leaved, deciduous" (1.04) and "Herbaceous Cover, closed-open" (1.04). Land cover class "Tree Cover, broadleaved, evergreen" has the lowest regression slope which is in accordance with the findings from region 5 (Fig. 6B 5). A 2.5% quantile regression slope value of  $-0.65$  indicates very large within-class variation. The same tendency is observed for "Mosaic: Cropland/Tree Cover/Other natural vegetation" (low regression slope (0.89) and 2.5% quantile value ( $-0.31$ )) which is to be expected since this class is predominantly located nearby "Tree Cover, broadleaved, evergreen". "Tree Cover, needle-leaved, evergreen" and "Tree Cover, broadleaved, deciduous, closed" also have regression slope values of  $<1$ . However, the low regression slope value for the class "Tree Cover, needle-leaved, evergreen" found in North America and Scandinavia as reported in Figs. 4C and 6B 2–3 is to some degree averaged out in the global cover class statistics in Table 3 since pixels belonging to this class in other areas (e.g. in southern USA and Russia) have regression slope values of  $>1$ .

## 5. Conclusions

The GIMMS global coverage dataset, spanning the period July 1981 to present, is currently the most widely used AVHRR based dataset for long term vegetation change studies. The accuracy of the long term GIMMS3g NDVI data was assessed using Terra MODIS NDVI (considered being state-of-the-art within high temporal global cover earth observation data) for an overlapping period of 11 years (2000–2010). It is concluded that the temporal trends derived from GIMMS NDVI are in overall good agreement with trends from MODIS NDVI data. A significant trend in NDVI ( $\alpha = 0.05$ ) was found for 11.8% of the MODIS pixels on a global scale whereas GIMMS NDVI analysis produced a total of 10.5% significant pixels. The spatial distribution of significantly positive and negative trends respectively agreed well for the Northern Hemisphere areas except for high arctic regions where MODIS data produces more pixels of positive NDVI trends compared to GIMMS. Larger discrepancies in trends were found for Southern Hemisphere continents, with MODIS and GIMMS NDVI trends disagreeing considerably for South America. The linear correlation between the two dataset was generally highly significant for areas with a clear phenological growth cycle. Comparing the GIMMS/MODIS NDVI correlation with the Terra/Aqua MODIS NDVI correlation provided a baseline for regions where less confidence may be had in NDVI trends from both GIMMS and MODIS data (primarily in high arctic regions and tropical rainforest areas). For the most sparsely vegetated areas with limited photosynthetic activity a

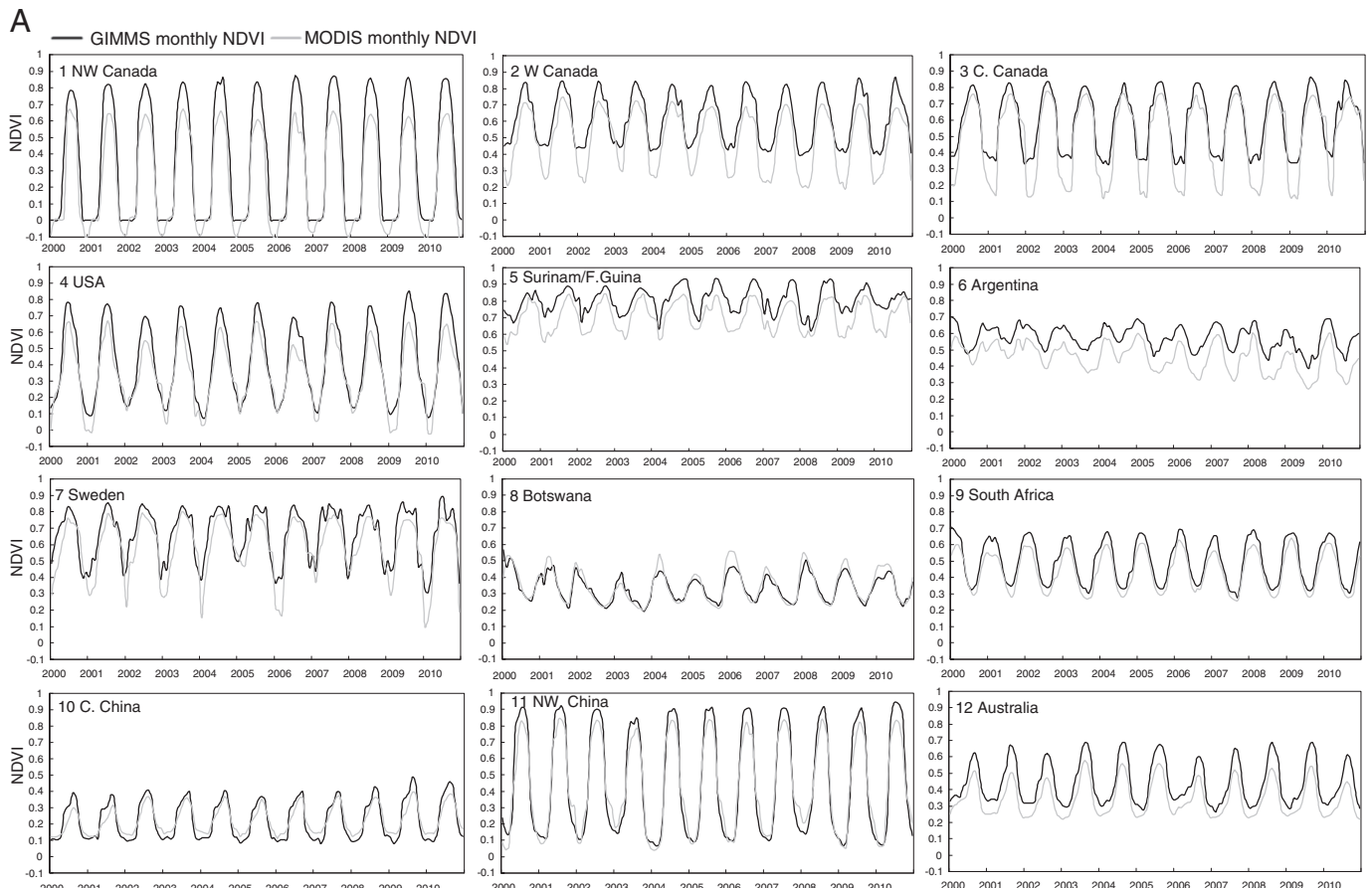


**Fig. 6.** (A) Time series of monthly GIMMS and MODIS NDVI (2000–2010) for selected regions (Fig. 4G) and (B) the corresponding scatterplots including regression slope, intercept and correlation coefficient. Pixels influenced from snow cover (Fig. 6A1) are excluded in the correlation analysis (Fig. 4) and in the Fig. 6B1 scatterplot.

B

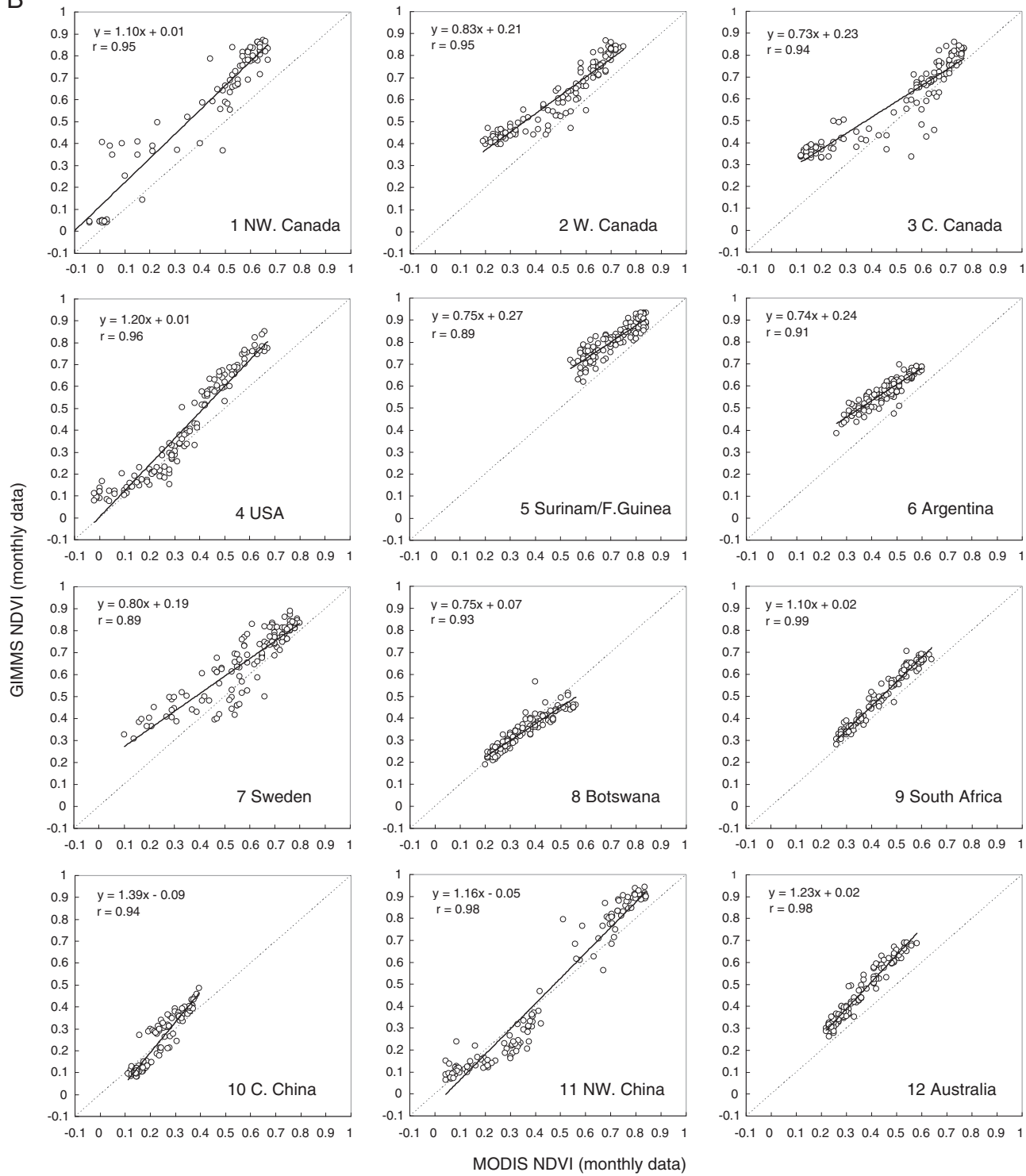


Fig. 6 (continued).

discrepancy between GIMMS and MODIS NDVI, not found between Terra and Aqua MODIS NDVI, suggests that trends in GIMMS data should be treated with caution.

For certain boreal regions deviations in the GIMMS/MODIS NDVI regression slope value from 1 was found to co-vary with land cover classes. "Needle-leaved evergreen forest" was found to have considerably lower winter MODIS NDVI as compared to GIMMS NDVI in North America and Scandinavia thereby producing differences in the regression slope values as compared to biomes with a different

vegetation structure such as the herbaceous cover classes and areas including cultivation. The differences found in the range of the MODIS and GIMMS NDVI co-varying with land cover classes must be studied further to determine the effect of land cover classes in the GIMMS sensor drift correction scheme based on empirical mode decomposition. In conclusion, this analysis suggests that GIMMS NDVI data form a relatively robust basis for detecting long-term trends in NDVI in most of the world's semi-arid, dry sub-humid and sub-humid areas.

**Table 3**

Statistics of the MODIS/GIMMS linear trend regression slope value ( $\alpha = 0.01$ ) for major land cover classes (GLC 2000).

| Land cover class (GLC 2000)                          | n         | n ( $\alpha = 0.01$ )% | regression slope value mean | 2.5% Quantile | 97.5% Quantile |
|--|-----------|------------------------|-----------------------------|---------------|----------------|
| Tree cover, broadleaved, evergreen                   | 143,207   | 35.6                   | 0.79                        | -0.65         | 1.92           |
| Tree cover, broadleaved, deciduous, closed           | 97,747    | 96.2                   | 1.01                        | 0.54          | 1.49           |
| Tree cover, broadleaved, deciduous, open             | 46,334    | 95.8                   | 0.93                        | 0.49          | 1.29           |
| Tree cover, needle-leaved, evergreen                 | 169,266   | 91.6                   | 0.97                        | 0.45          | 1.82           |
| Tree cover, needle-leaved, deciduous                 | 92,460    | 95.9                   | 1.04                        | 0.54          | 1.64           |
| Tree cover, mixed leaf type                          | 63,629    | 96.6                   | 1.01                        | 0.56          | 1.73           |
| Mosaic: Tree cover/other natural vegetation          | 48,206    | 89.4                   | 1.10                        | 0.55          | 2.09           |
| Shrub cover, closed-open, evergreen                  | 35,129    | 83.1                   | 1.06                        | 0.47          | 1.98           |
| Shrub cover, closed-open, deciduous                  | 169,543   | 91.3                   | 0.98                        | 0.46          | 1.73           |
| Herbaceous cover, closed-open                        | 191,442   | 94.1                   | 1.04                        | 0.49          | 1.84           |
| Sparse herbaceous or sparse shrub cover              | 203,658   | 77.4                   | 1.11                        | 0.39          | 2.22           |
| Regularly flooded shrub and/or herbaceous cover      | 34,015    | 90.3                   | 1.05                        | 0.49          | 1.93           |
| Cultivated and managed areas                         | 238,918   | 94.5                   | 1.02                        | 0.50          | 1.56           |
| Mosaic: Cropland/tree cover/other natural vegetation | 43,745    | 67.2                   | 0.89                        | -0.31         | 1.65           |
| Mosaic: Cropland/shrub and/or grass cover            | 44,232    | 97.5                   | 1.02                        | 0.57          | 1.52           |
| All classes  | 1,758,745 | 86.4                   | 1.00                        | 0.37          | 1.76           |

## Acknowledgement

The author thanks the NASA Global Inventory Modelling and Mapping Studies (GIMMS) group for producing and sharing the GIMMS3g NDVI dataset. NASA/MODIS Land Discipline Group is thanked for sharing the MODIS LAND data. Finally, the reviewers are thanked for their many constructive comments and suggestions.

## References

- Alcaraz-Segura, D., Chuvieco, E., Epstein, H. E., Kasischke, E. S., & Trishchenko, A. (2010). Debating the greening vs. browning of the North American boreal forest: Differences between satellite datasets. *Global Change Biology*, 16, 760–770.
- Alcaraz-Segura, D., Liras, E., Tabik, S., Paruelo, J., & Cabello, J. (2010). Evaluating the consistency of the 1982–1999 NDVI trends in the Iberian Peninsula across four time-series derived from the AVHRR sensor: LTDR, GIMMS, FASIR, and PAL-II. *Sensors*, 10(2), 1291–1314.
- Anyamba, A., & Tucker, C. J. (2005). Analysis of Sahelian vegetation dynamics using NOAA-AVHRR NDVI data from 1981–2003. *Journal of Arid Environments*, 63, 596–614.
- Bartholomé, E., Belward, A. S., Achard, F., Bartalev, S., Carmona-Moreno, C., Eva, H., et al. (2002). GLC 2000: Global Land Cover mapping for the year 2000, EUR 20524 EN. Luxembourg: European Commission.
- Beck, P. S. A., & Goetz, S. J. (2011). Satellite observations of high northern latitude vegetation productivity changes between 1982 and 2008: Ecological variability and regional differences. *Environmental Research Letters*, 6, 045501.
- Beck, H. E., McVicar, T. R., van Dijk, A. I. J. M., Schellekens, J., de Jeu, R. A. M., & Bruijnzeel, L. A. (2011). Global evaluation of four AVHRR-NDVI data sets: Intercomparison and assessment against Landsat imagery. *Remote Sensing of Environment*, 115, 2547–2563.
- Brando, P. M., Goetz, S. J., Baccini, A., Nepstad, D. C., Beck, P. S. A., & Christman, M. C. (2010). Seasonal and interannual variability of climate and vegetation indices across the Amazon. *Proceedings of the National Academy of Sciences of the United States of America*, 107, 14685–14690.
- Brown, M. E., Pinzon, J. E., Didan, K., Morisette, J. T., & Tucker, C. J. (2006). Evaluation of the consistency of long-term NDVI time series derived from AVHRR, SPOT-Vegetation, SeaWiFS, MODIS, and Landsat ETM + sensors. *IEEE Transactions on Geoscience and Remote Sensing*, 44, 1787–1793.
- Cihlar, J., Tcherednichenko, I., Latifovic, R., Li, Z., & Chen, J. (2001). Impact of variable atmospheric water vapor content on AVHRR data corrections over land. *IEEE Transactions on Geoscience and Remote Sensing*, 39, 173–180.
- Cracknell, A. P. (2001). The exciting and totally unanticipated success of the AVHRR in applications for which it was never intended. *Calibration and Characterization of Satellite Sensors and Accuracy of Derived Physical Parameters*, 28, 233–240.
- de Beurs, K. M., & Henebry, G. M. (2005). Land surface phenology and temperature variation in the International Geosphere-Biosphere Program high-latitude transects. *Global Change Biology*, 11, 779–790.
- de Jong, R., de Bruin, S., de Wit, A., Schaepman, M. E., & Dent, D. L. (2011). Analysis of monotonic greening and browning trends from global NDVI time-series. *Remote Sensing of Environment*, 115, 692–702.
- Eastman, J. R., Sangermano, F., Ghimire, B., Zhu, H. L., Chen, H., Neeti, N., et al. (2009). Seasonal trend analysis of image time series. *International Journal of Remote Sensing*, 30, 2721–2726.
- Eklundh, L., & Olsson, L. (2003). Vegetation index trends for the African Sahel 1982–1999. *Geophysical Research Letters*, 30.
- Fensholt, R., Nielsen, T. T., & Stisen, S. (2006). Evaluation of AVHRR PAL and GIMMS 10-day composite NDVI time series products using SPOT-4 vegetation data for the African continent. *International Journal of Remote Sensing*, 27, 2719–2733.
- Fensholt, R., & Rasmussen, K. (2011). Analysis of trends in the Sahelian ‘rain-use efficiency’ using GIMMS NDVI, RFE and GPCP rainfall data. *Remote Sensing of Environment*, 115, 438–451.
- Fensholt, R., Rasmussen, K., Nielsen, T. T., & Mbow, C. (2009). Evaluation of earth observation based long term vegetation trends – Intercomparing NDVI time series trend analysis consistency of Sahel from AVHRR GIMMS, Terra MODIS and SPOT VGT data. *Remote Sensing of Environment*, 113, 1886–1898.
- Fensholt, R., & Sandholt, I. (2005). Evaluation of MODIS and NOAA AVHRR vegetation indices with in situ measurements in a semi-arid environment. *International Journal of Remote Sensing*, 26, 2561–2594.
- Fensholt, R., Sandholt, I., & Stisen, S. (2006). Evaluating MODIS, MERIS, and VEGETATION – Vegetation indices using in situ measurements in a semiarid environment. *IEEE Transactions on Geoscience and Remote Sensing*, 44, 1774–1786.
- Goward, S. N., Dye, D. G., Turner, S., & Yang, J. (1993). Objective assessment of the NOAA Global Vegetation Index data product. *International Journal of Remote Sensing*, 14, 3365–3394.
- Hellden, U., & Tottrup, C. (2008). Regional desertification: A global synthesis. *Global and Planetary Change*, 64, 169–176.
- Herrmann, S. M., Anyamba, A., & Tucker, C. J. (2005). Recent trends in vegetation dynamics in the African Sahel and their relationship to climate. *Global Environmental Change-Human and Policy Dimensions*, 15, 394–404.
- Heumann, B. W., Sequist, J. W., Eklundh, L., & Jonsson, P. (2007). AVHRR derived phenological change in the Sahel and Sudan, Africa, 1982–2005. *Remote Sensing of Environment*, 108, 385–392.
- Hickler, T., Eklundh, L., Sequist, J. W., Smith, B., Ardo, J., Olsson, L., et al. (2005). Precipitation controls Sahel greening trend. *Geophysical Research Letters*, 32.
- Hirsch, R. M., & Slack, J. R. (1984). A nonparametric trend test for seasonal data with serial dependence. *Water Resources Research*, 20, 727–732.
- Hoaglin, D. C., Mosteller, F., & Tukey, J. W. (2000). *Understanding robust and exploratory data analysis*. New York: Wiley.
- Holben, B. N. (1986). Characteristics of maximum-value composite images from temporal AVHRR data. *International Journal of Remote Sensing*, 7, 1417–1434.
- Huete, A., Didan, K., Miura, T., Rodriguez, E. P., Gao, X., & Ferreira, L. G. (2002). Overview of the radiometric and biophysical performance of the MODIS vegetation indices. *Remote Sensing of Environment*, 83, 195–213.
- Huete, A. R., Liu, H. Q., & Van Leeuwen, W. J. D. (1997). The use of vegetation indices in forested regions: issues of linearity and saturation. *Proceedings of IGARSS' 97-International Geoscience and Remote Sensing Seminar* (pp. 1966–1968). Noordwijk: ESA Publications.
- Ignatov, A., Laszlo, I., Harrod, E. D., Kidwell, K. B., & Goodrum, G. P. (2004). Equator crossing times for NOAA, ERS and EOS sun-synchronous satellites. *International Journal of Remote Sensing*, 25, 5255–5266.
- James, M. E., & Kalluri, S. N. V. (1994). The Pathfinder AVHRR Land Data Set – An improved coarse resolution data set for terrestrial monitoring. *International Journal of Remote Sensing*, 15, 3347–3363.
- Jeyaseelan, A. T., Roy, P. S., & Young, S. S. (2007). Persistent changes in NDVI between 1982 and 2003 over India using AVHRR GIMMS (global inventory Modeling and mapping studies) data. *International Journal of Remote Sensing*, 28, 4927–4946.
- Jonsson, P., & Eklundh, L. (2002). Seasonality extraction by function fitting to time-series of satellite sensor data. *IEEE Transactions on Geoscience and Remote Sensing*, 40, 1824–1832.
- Jonsson, P., & Eklundh, L. (2004). TIMESAT – A program for analyzing time-series of satellite sensor data. *Computers & Geosciences*, 30, 833–845.
- Justice, C. O., Vermote, E., Townsend, J. R. G., Defries, R., Roy, D. P., Hall, D. K., et al. (1998). The Moderate Resolution Imaging Spectroradiometer (MODIS): Land remote sensing for global change research. *IEEE Transactions on Geoscience and Remote Sensing*, 36, 1228–1249.
- Kidwell, K. B. (1991). *NOAA Polar Orbiter data user's guide*. Washington, DC: NCDC/SDSD, National Climatic Data Center.
- Los, S. O. (1998). Estimation of the ratio of sensor degradation between NOAA AVHRR channels 1 and 2 from monthly NDVI composites. *IEEE Transactions on Geoscience and Remote Sensing*, 36, 206–213.

- Los, S. O., Collatz, G. J., Sellers, P. J., Malmstrom, C. M., Pollack, N. H., DeFries, R. S., et al. (2000). A global 9-yr biophysical land surface dataset from NOAA AVHRR data. *Journal of Hydrometeorology*, 1(2), 183–199.
- Myneni, R. B., Keeling, C. D., Tucker, C. J., Asrar, G., & Nemani, R. R. (1997). Increased plant growth in the northern high latitudes from 1981 to 1991. *Nature*, 386, 698–702.
- Myneni, R. B., Tucker, C. J., Asrar, G., & Keeling, C. D. (1998). Interannual variations in satellite-sensed vegetation index data from 1981 to 1991. *Journal of Geophysical Research – Atmospheres*, 103, 6145–6160.
- Nagol, J. R., Vermote, E. F., & Prince, S. D. (2009). Effects of atmospheric variation on AVHRR NDVI data. *Remote Sensing of Environment*, 113, 392–397.
- Nemani, R. R., Keeling, C. D., Hashimoto, H., Jolly, W. M., Piper, S. C., Tucker, C. J., et al. (2003). Climate-driven increases in global terrestrial net primary production from 1982 to 1999. *Science*, 300, 1560–1563.
- Olsson, L., Eklundh, L., & Ardo, J. (2005). A recent greening of the Sahel – Trends, patterns and potential causes. *Journal of Arid Environments*, 63, 556–566.
- Pedelty, J., Devadiga, S., Masuoka, E. B., Pinzon, J. M., Tucker, C. J., Vermote, E. F., et al. (2007). Generating a long-term land data record from the AVHRR and MODIS Instruments. *Geoscience and Remote Sensing Symposium, 2007. IGARSS 2007. IEEE International* (pp. 1021–1025).
- Pinzon, J. E., Brown, M. E., & Tucker, C. J. (2007). Global Inventory Modeling and Mapping Studies (GIMMS) satellite drift corrected and NOAA-16 incorporated Normalized Difference Vegetation Index (NDVI), monthly 1981–2006. [http://www.glcf.umd.edu/library/guide/GIMMSdocumentation\\_NDVIg\\_GLCF.pdf](http://www.glcf.umd.edu/library/guide/GIMMSdocumentation_NDVIg_GLCF.pdf)
- Pinzon, J.E., Brown, M.E., & Tucker, C.J. (2005). Hilbert-Huang transform and its applications. In N.E. Huang (Ed.), *Interdisciplinary mathematical sciences v. 5* (pp. xii, 311 p.). Singapore; Hackensack, NJ; London: World Scientific.
- Prince, S. D., & Goward, S. N. (1995). Global primary production: A remote sensing approach. *Journal of Biogeography*, 22, 815–835.
- Rouse, J. W., Hass, R. H., Schell, J. A., & Deering, D. W. (1973). Monitoring vegetation systems in the Great Plains with ERTS. *3rd ERTS symposium* (pp. 309–317). Washington DC: U.S. Government Printing Office (ed. SP-351).
- Ruimy, A., Saugier, B., & Dedieu, G. (1994). Methodology for the estimation of terrestrial net primary production from remotely sensed data. *Journal of Geophysical Research – Atmospheres*, 99, 5263–5283.
- Saleska, S. R., Didan, K., Huete, A. R., & da Rocha, H. R. (2007). Amazon forests green-up during 2005 drought. *Science*, 318, 612.
- Samanta, A., Ganguly, S., Hashimoto, H., Devadiga, S., Vermote, E., Knyazikhin, Y., et al. (2010). Amazon forests did not green-up during the 2005 drought. *Geophysical Research Letters*, 37.
- Slaback, D. A., Pinzon, J. E., Los, S. O., & Tucker, C. J. (2003). Northern Hemisphere photosynthetic trends 1982–99. *Global Change Biology*, 9, 1–15.
- Solano, R., Didan, K., Jacobson, A., & Huete, A. (2010). MODIS Vegetation Indices (MOD13) C5 user's guide. Available at: <http://tbrs.arizona.edu/project/MODIS/UsersGuide.pdf>
- Steven, M. D., Malthus, T. J., Baret, F., Xu, H., & Chopping, M. J. (2003). Intercalibration of vegetation indices from different sensor systems. *Remote Sensing of Environment*, 88, 412–422.
- Stisen, S., Sandholt, I., Norgaard, A., Fensholt, R., & Eklundh, L. (2007). Estimation of diurnal air temperature using MSG SEVIRI data in West Africa. *Remote Sensing of Environment*, 110, 262–274.
- Stockli, R., & Vidale, P. L. (2004). European plant phenology and climate as seen in a 20-year AVHRR land-surface parameter dataset. *International Journal of Remote Sensing*, 25, 3303–3330.
- Stowe, L. L., McClain, E. P., Carey, R., Pellegrino, P., Gutman, G. G., Davis, P., et al. (1991). Global distribution of cloud cover derived from NOAA/AVHRR operational satellite data. *Advances in Space Research*, 3, 51–54.
- Swinnen, E., & Veroustraete, F. (2008). Extending the SPOT-VEGETATION NDVI time series (1998–2006) back in time with NOAA-AVHRR data (1985–1998) for southern Africa. *IEEE Transactions on Geoscience and Remote Sensing*, 46, 558–572.
- Tanré, D., Holben, B. N., & Kaufman, Y. J. (1992). Atmospheric correction algorithm for NOAA-AVHRR products: Theory and application. *IEEE Transactions on Geoscience and Remote Sensing*, 30(2), 231–248.
- Teillet, P. M., Staenz, K., & Williams, D. J. (1997). Effects of spectral, spatial, and radiometric characteristics on remote sensing vegetation indices of forested regions. *Remote Sensing of Environment*, 61, 139–149.
- Thorne, P. W., Lanzante, J. R., et al. (2011). Tropospheric temperature trends: History of an ongoing controversy. *Wiley Interdisciplinary Reviews: Climate Change*, 2(1), 66–88.
- Townshend, J. R. G. (1994). Global Data Sets for land applications from the Advanced Very High-Resolution Radiometer – An introduction. *International Journal of Remote Sensing*, 15, 3319–3332.
- Tucker, C. J., Pinzon, J. E., Brown, M. E., Slayback, D. A., Pak, E. W., Mahoney, R., et al. (2005). An extended AVHRR 8-km NDVI dataset compatible with MODIS and SPOT vegetation NDVI data. *International Journal of Remote Sensing*, 26, 4485–4498.
- Tucker, C. J., Slayback, D. A., Pinzon, J. E., Los, S. O., Myneni, R. B., & Taylor, M. G. (2001). Higher northern latitude normalized difference vegetation index and growing season trends from 1982 to 1999. *International Journal of Biometeorology*, 45, 184–190.
- Tucker, C. J., Vanpraet, C., Boerwinkel, E., & Gaston, A. (1983). Satellite remote-sensing of total dry-matter production in the Senegalese Sahel. *Remote Sensing of Environment*, 13, 461–474.
- van Leeuwen, W. J. D., Huete, A. R., & Laing, T. W. (1999). MODIS vegetation index compositing approach: A prototype with AVHRR data. *Remote Sensing of Environment*, 69, 264–280.
- Vanbeloe, G., & Hughes, J. P. (1984). Nonparametric-tests for trend in water-quality. *Water Resources Research*, 20, 127–136.
- Vermote, E. F., El Saleous, N. Z., & Justice, C. O. (2002). Atmospheric correction of MODIS data in the visible to middle infrared: First results. *Remote Sensing of Environment*, 83, 97–111.
- Vermote, E., & Kaufman, Y. J. (1995). Absolute calibration of AVHRR visible and near-infrared channels using ocean and cloud views. *International Journal of Remote Sensing*, 16, 2317–2340.
- Wolfe, R. E., Roy, D. P., & Vermote, E. (1998). MODIS land data storage, gridding, and compositing methodology: Level 2 grid. *IEEE Transactions on Geoscience and Remote Sensing*, 36, 1324–1338.
- Xiao, X. M., Braswell, B., Zhang, Q. Y., Boles, S., Frolking, S., & Moore, B. (2003). Sensitivity of vegetation indices to atmospheric aerosols: Continental-scale observations in Northern Asia. *Remote Sensing of Environment*, 84, 385–392.
- Zeng, G., Wang, Z., Wen, S., Jiang, J., Wang, L., Cheng, J., et al. (2005). Geographic distribution, virologic and clinical characteristics of hepatitis B virus genotypes in China. *Journal of Viral Hepatitis*, 12, 609–617.
- Zhou, L., Tucker, C. J., Kaufmann, R. K., Slayback, D., Shabanov, N. V., & Myneni, R. B. (2001). Variations in northern vegetation activity inferred from satellite data of vegetation index during 1981 to 1999. *Journal of Geophysical Research*, 106(17), 20,069–20,083.